Climatology of Medium-Scale Traveling Ionospheric Disturbances (MSTIDs) Observed with GPS Networks in the North African Region

Oluwadare T. Seun.
Institut fur Geodasie und Geoinformationstechnik, Technische Universitat Berlin,Str. des 17. Juni 135, 10623, Berlin, Germany. German Research Centre for Geosciences GFZ, Telegrafenberg, D-14473 Potsdam, Germany.
oluwa@gfz-potsdam.de , temitopeseun@yahoo.co.uk

Norbert Jakowski.
German Aerospace Center (DLR), Institute of Communications and Navigation, Ionosphere Group, Kalkhorstweg 53, 17235 Neustrelitz, Germany
Norbert.Jakowski@dlr.de

Cesar E. Valladares.
W.B Hanson Center for Space Sciences, University of Texas at Dallas, USA
Cesar.Valladares@utdallas.edu

Andrew Oke-Ovie Akala
Department of Physics, University of Lagos, Akoka, Yaba, Lagos, Nigeria
aakala@unilag.edu.ng

Oladipo E. Abe
Physics Department, Federal University Oye-Ekiti, Nigeria
oladipo.abe@fuoye.edu.ng

Mahdi M. Alizadeh
Faculty of Geodesy and Geomatics Engineering, K.N. Toosi, University of Technology, Tehran, Iran. Institut fur Geodasie und Geoinformationstechnik, Technische Universitat Berlin,Str. des 17. Juni 135, 10623, Berlin, Germany.
m.alizadeh@email.com

Harald Schuh.
Institut fur Geodasie und Geoinformationstechnik, Technische Universitat Berlin,Str. des 17. Juni 135, 10623, Berlin, Germany. German Research Centre for Geosciences GFZ, Telegrafenberg, D-14473 Potsdam, Germany.
schuh@gfz-potsdam.de

Climatology of Medium-Scale Traveling Ionospheric Disturbances (MSTIDs) Observed with GPS Networks in the North African Region

Oluwadare T. Seun[1, 2], Norbert Jakowski[3], Cesar E. Valladares[4], Andrew O. Akala[5], Oladipo E. Abe[6], Mahdi M. Alizadeh[1,7], Harald Schuh[1, 2]

[1]Institut fur Geodasie und Geoinformationstechnik, Technische Universitat Berlin,Str. des 17, 10623, Berlin, Germany
[2]German Research Centre for Geosciences GFZ, Telegrafenberg, D-14473 Potsdam, Germany
[3]German Aerospace Center (DLR), Institute of Communications and Navigation, Ionosphere Group, Neustrelitz, Germany
[4]W.B Hanson Center for Space Sciences, University of Texas at Dallas, USA
[5]Department of Physics, University of Lagos, Akoka, Yaba, Lagos, Nigeria
[6]Department of Physics, Federal University, Oye-Ekiti, Nigeria
[7]Faculty of Geodesy and Geomatics Engineering, K.N. Toosi, University of Technology,Tehran, Iran.

Abstract

We present for the first time the climatology of medium-scale traveling ionospheric disturbances (MSTIDs) by using Global Positioning System (GPS) receiver networks on geomagnetically quiet days (Kp ≤ 3) over the North African region during 2008-2016. The MSTIDs appear frequently as oscillating waves or wave-like structures in electron density induced by the passage of Atmospheric Gravity Waves (AGW) propagating through the neutral atmosphere and consequently, causing fluctuation in the ionospheric Total Electron Content (TEC). The TEC perturbations (dTEC) data are derived from dual frequency GPS-measurements. We have statistically analyzed the occurrence rate, diurnal and seasonal behavior as well as the annual MSTID occurrence characteristics. The results show a local and latitude dependence of nighttime and daytime MSTIDs. The propagation direction is predominantly towards the South (equatorward), MSTIDs event period is (10 ≤ period ≤ 43 mins), and amplitude (0.08 ≤ amp ≤ ~5.0 TECU), with a velocity higher at nighttime than daytime. The amplitudes for daytime and nighttime MSTIDs increase with solar activity. On the average, the local MSTIDs Spatio-temporal heat map for the Mid-latitude reveals variability in disturbance occurrence time to be dominant within the hours of 0900 - 1600 LT in December solstice (winter) and 1900–0400 LT in June solstice (summer) for daytime and nighttime respectively. While the low latitude reveals the disturbance occurrence time to be dominant within the hours of 1100 - 1800 LT in December solstice (winter) and 2000–0200 LT in equinox months and June solstice (summer) for daytime and nighttime respectively. The time series MSTIDs regional distribution map is also generated. Atmospheric gravity waves (AGW) might be responsible for the excitation mechanism for daytime MSTIDs.

Keywords: Medium scale traveling ionospheric disturbances, ionospheric irregularities, Atmospheric Gravity Waves, Total Electron Content

1.0 Introduction.

Medium-scale traveling ionospheric disturbance (MSTID) is one of the major and frequent ionospheric irregularity phenomena at the F region Mid-latitude which may degrade positioning systems and it has been studied to have the ability to propagate over long distances (Frissell et al., 2014). Medium-scale traveling ionospheric disturbances (MSTIDs) could degrade the signals propagating through the ionosphere and sometimes result to loss of signals to both communication and navigation systems. The MSTIDs frequently appear as oscillating waves in electron density induced by the passage of atmospheric gravity waves (AGW) propagating upward from the lower atmospheric regions (Fedorenko et al., 2010). The AGWs is predominantly assumed to be launched by the solar terminator (Kotake et al., 2007), have been linked to mid-latitude MSTID observations. AGWs are the most impactful waves that contribute to the dynamical nature of the upper atmosphere amongst many waves present in the atmosphere, and it is also an important energy transfer mechanism from troposphere into the stratosphere, mesosphere, and thermosphere (Jia Yue et al., 2019). AGW manifest as a wave-like perturbation of ionospheric plasma in the ionosphere (Hines, 1960), consequently causing fluctuations in Total Electron Content (TEC). The AGW propagation through the neutral atmosphere eventually gets above 50 km into the ionosphere and directly impacts it, causing ionospheric variability and seeds ionospheric irregularities (Azeem and Barlage, 2017) such as MSTIDs. These entire ionospheric frequent phenomena consequently cause fluctuations in Total Electron Content (TEC). The daytime MSTIDs event occurrence is majorly assumed to be caused by atmospheric gravity waves (AGW), (Hines, 1960; Jonah et al., 2016; Oinats et al., 2016; Figueiredo et al., 2018), while the nighttime is assumed to be caused by electrodynamical forces such as Perkins instability respectively (Perkins, 1973; Garcia et al., 2000; Tsugawa et al., 2007). The wavelike structure of MSTIDs is characterized by a wavelength, period and phase speed of 50 - 500 km, 12 - 60 mins and 50–400 m/s, respectively (Ogawa et al., 1987; Hocke and Schlegel, 1996; Grocott et al., 2013). Within the last six decades, a lot of MSTIDs studies have been carried out by various researchers around the globe using different instruments and techniques to understand this irregular ionospheric behaviour. To mention a few amongst many are: Ogawa et al. (1987) who investigated MSTIDs occurrence frequency using the U.S. Navy Navigation Satellite System (NNSS) in polar region at a 1000 km altitude during the disturbed geomagnetic condition. The authors concluded that there was no increase in MSTIDs occurrence under disturbed condition. Hernández-Pajares et al. (2006, 2012), Kotake et al. (2007), Valladares and Hei, (2012), Jonah et al. (2016), Figueiredo et al. (2018), and Guanyi Chen et al. (2019) carried out independent research of MSTIDs using GNSS receiver network at difference location and they reported nearly the same results in terms of seasonal occurrences, but with slight differences in the propagation directions. Oinats et al. (2016) used Super Dual Auroral Radar Network (SuperDARN) high frequency (HF) radar data and reported that MSTIDs increases with solar activity, while Jacobson et al. (1995) used satellite – beacon

radio interferometer and concluded that daytime MSTIDs propagate mainly southward, while the nighttime MSTIDs propagate southwestward. Many studies have reported the regular and dynamic nature of the ionospheric TEC at different latitudes over the African region (Ouattara and Fleury, 2011; Ngwira et al., 2013; D'ujanga et al., 2016) but these earlier studies have only been confined to short-term time basis observation under limited solar activity. Besides, the majority of the investigations reported to date have mostly emphasized the local or regional characteristics of ionospheric irregularities with main focus on scintillation. However, there is yet an important aspect of ionospheric irregularities which is yet to be reported on both local and regional scale over Africa. In recent years, with an improved study of long- term time series of characterization of ionospheric GPS-TEC under different geomagnetic conditions for daytime and nighttime, respectively, during 2009 – 2016 (Oluwadare et al., 2018), certain wave-like structures of ionospheric TEC were observed to be irregularities which vary in time and space. The characteristics of this irregular phenomenon are mostly associated with MSTIDs as described by ionospheric irregularity theories and experimental results from different authors who have reported MSTIDs observations from different regions e.g. North Asia, South America, North America, Europe, and Oceania around the globe except for the African region, and these have created a huge gap in comparison of interregional MSTIDs characteristics. Before now, MSTIDs study over the African region has not been reported, probably due to limitation of ionospheric data availability in the non-African region or none-access to the GPS data and other technical reasons. Hence, this study has considered further observing and investigating the dynamic nature of ionosphere and the occurrence of ionospheric irregularities with main focus on MSTIDs from GPS-TEC estimates. The study investigates the climatology of MSTIDs over the North African region for the first time during the geomagnetic quiet days (i.e. $Kp \leq 3$) for the period of nine years (2008-2016). The primary aim is to present the MSTIDs observations derived from estimated TEC perturbation (dTEC), characteristics and occurrence mechanism. We also show the perturbed temperature profile as tropospheric activities obtained from the Constellation Observing System for Meteorology, Ionosphere, and Climate (COSMIC) satellite which exhibits AGW signature and widely thought to be majorly due to the vertical propagation of AGW (Grant et al., 1998). For the first time, we present the nine years' climatology of MSTIDs observed by a GPS network over the North African region. The MSTIDs occurrence rate (OR) is estimated, its characteristics as well as the mechanisms are investigated. In addition, the regional distribution of MSTIDs occurrence map is presented and a daytime two-dimensional dTEC map for a case of MSTIDs was also presented.

2.0 Instrumentation and data description

MSTIDs have been observed and estimated during 2008-2016 using seven ground-based dual-frequency GPS receiver network stations majorly situated at Northern African, a mid-latitude region. The location of

the stations are: Rabat (RABT: 33.99°N, 6.85°W, mag. lat: 37.4°N); Tetouan (TETN; 35.56°N, 5.36°W, mag. lat: 38.6°N); Ifrane (IFR1: 33.51°N, 5.13°W, mag. lat: 36.7°N); Noto (NOT1: 36.88°N, 14.91°E, mag. lat: 36.5°N); Alexandria (ALX2: 31.20°N, 29.91°E, mag. lat: 28.5°N); Cyprus (NICO: 35.14°N, 33.40°E, mag. lat: 31.8°N); Ramon (RAMO; 30.60°N, 34.76°E, mag. lat: 27.1°N) and one station situated at the low latitude; Maspalomas (MAS1: 27.76°N, 15.63°W, mag. lat: 19.8°N). The entire eight GPS network stations are shown in Fig. 1.

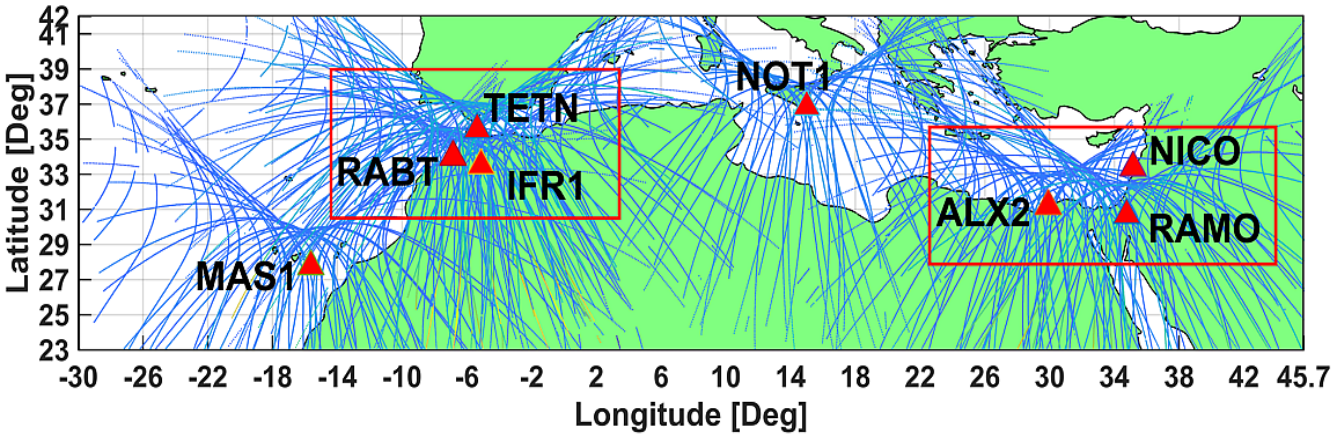

Fig. 1 Location of the GPS receiver stations (red triangles) used in this study with an elevation mask ≥ 35^0. GPS geometric networks were formed by choosing minimum of three stations (enclosed in red box) to form new sub networks (N1: RABT-TETN-IFR1, N2: ALX2-NICO-RAMO)

The observation GPS data in Rinex format were obtained from the following FTP sites: ftp://data-out.unavco.org/pub/rinex/, ftp://igs.ign.fr/pub/igs/data/, http://www.afrefdata.org/ and ftp://www.station-gps.cea.com.eg/ALX2/, respectively. The GPS distribution is presented with red triangle with the corresponding IPP trajectory (blue color curve) of the GPS satellites (Fig. 1). To avoid water vapor scattering multipath effects and effect from the mapping function uncertainty from the data, an elevation cut-off angle greater than 35^0 (Bagiya et al., 2009; Valladares and Hei, 2012) was adopted.

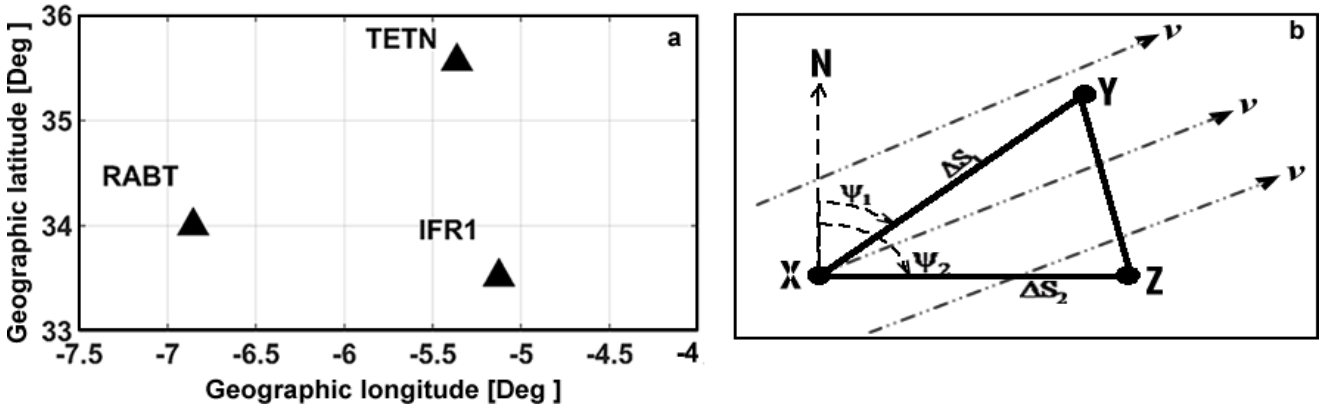

Fig. 2 (a) An example illustrating one of the sub-networks (N1: RABT-TETN-IFR1) used in studying MSTIDs characteristics. (b) The configured network geometry for obtaining the MSTIDs propagation direction and velocity.

Also the low geomagnetic activity conditions were considered using K planetary (Kp) index. The magnitude of Kp index ≤ 3 was considered for low geomagnetic quiet conditions during the study period. The Kp index data were obtained from the GFZ German Research Centre for Geosciences, Indices of Global Geomagnetic Activity, Potsdam, Germany (ftp://ftp.gfz-potsdam.de/pub/home/obs/kp-ap). Days with Kp ≤ 3 during 2008-2016 were filtered out and used for this study. Furthermore, we made use of temperature profile data extracted from the COSMIC satellite. The COSMIC satellites is a low Earth orbit (LEO) satellite that provides both upper and lower atmospheric products for different altitude observations of temperature, the electron density of the ionosphere, pressure, refractivity, and water vapor. We extracted and observed some perturbed temperature profile which may be due to the vertical propagation of AGWs from the COSMIC data (Grant et al., 1998). We made use of the temperature profile measurements that is closest to the GPS station. COSMIC data are available at COSMIC Data Analysis and Archive Center (CDAAC) website (https://cdaac-www.cosmic.ucar.edu/cdaac/tar/rest.html).

3.0 Estimation of MSTIDs Characteristics from GPS-TEC

The ionospheric total electron content (TEC) used in this study is computed from the dual frequency GPS receiver consisting of both code (pseudorange) and carrier phase observations transmitting on L1 (f1=1575.42 MHz) and L2 (f2=1227.60 MHz) frequencies. Measurements are taken at 30 seconds interval. Code (pseudorange) and carrier phase measurements are denoted as Pi and ϕ_i (i = 1, 2) (Gao and Liu, 2002). The GPS frequencies experience different group delays and phase advances due to the dispersive nature of ionosphere, see (equ. (1)).

$$I = \pm \frac{40.3}{f^2} TEC \tag{1}$$

were f is the signal frequency (Hz), (+) corresponds to group delay while (-) corresponds to carrier delay, (Pratap and Enge, 2006). The difference between the code (pseudorange) (P_i) and carrier phases (ϕ_i) respectively are computed. Observation equations for both code (pseudorange) and carrier phase on L_1 and L_2 are formed.

$$P_i = \rho + c(\Delta t_r - \Delta t_s) + T + I_i + b_{ir}^P + b_{is}^P + m_i^P + \varepsilon_i^P \tag{2}$$

$$L_i = \rho + c(\Delta t_r - \Delta t_s) + T - I_i + \lambda_i N_i + m_i^L + \varepsilon_i^L \tag{3}$$

where subscripts *r, s*, and *i,* implies receiver, satellite and GPS frequency number, respectively. P_i is the slant range between satellite and receiver, ρ is geometric range (distance) between receiver and satellite, (b^P_{ir}, b^P_{is}) receiver and satellite hardware delay/biases expressed in time (sec) unit respectively (i.e. regarded as differential code biases (DCB)), m_i, is multi-path effect (m), ε_i is the measurement noise (m), I_i is the

ionospheric delay (frequency dependence), T is signal delay due to the troposphere, (Δt_r, Δt_s) is the receiver and satellite clock error with respect to GPS time (sec), and $\lambda_i N_i$ are the integer phase ambiguity. Equation (1) is substituted into equ (2) and resolve. The geometry-related parameters are eliminated, and then we obtain equ (4 and 5)

$$P_1 - P_2 = (I_1 - I_2) + c(\Delta b_s - \Delta b_r) \tag{4}$$

$$TEC_p = \frac{1}{40.3}\left(\frac{f_1^2 f_2^2}{f_1^2 - f_2^2}\right)(P_1 - P_2) \tag{5}$$

The TEC extracted from the code (pseudorange) measurements (TECP) are noisier but are free from any integer ambiguity, the carrier phase observations from L1 and L2 described in equ. (3) was used to smooth the code observation for a more precise STEC estimate (Zhao et al., 2009). We correct for the effect of DCB on the GNSS raw data in order to obtain absolute STEC. The DCB values were obtained from ftp server (ftp://ftp.unibe.ch/aiub/CODE). As STEC is dependent on the ray path geometry through the ionosphere, it is needful to calculate an equivalent vertical TEC (VTEC) value which is independent of the elevation of the ray path. The VTEC is obtained by taking the projection from the slant to vertical using a mapping function model (M) of the below relation (equ. (6)), assuming a height of 350 km, following the technique given by (Klobuchar, 1986).

$$M(\theta) = \frac{VTEC}{STEC} = \left[1 - \left(\frac{R_e \cos(\theta)}{R_e + h_{\max}}\right)^2\right]^{\frac{1}{2}} \tag{6}$$

where Re is the mean earth radius; 6371 km, hmax is the altitude of the thin layer above the surface of the Earth, θ = elevation angle of the satellite in degrees (Mannucci et al., 1993; Langley et al., 2002), 350 km, has been taken to be h_{max} value, this is because at this height the ionosphere is assumed to be spatially uniform and simplified to be a thin layer, hence, this is considered as the height of maximum electron density at the F2 peak (Mannucci et al., 1998; Norsuzila et al., 2009). More details about TEC estimation can be found in Mannucci et al. (1998) and Ciraolo L. et al (2006). The background trends of the TEC time series were obtained by using singular spectrum analysis (SSA) with sliding window duration of 60 mins and thereafter the output is subtracted from the original TEC time series resulting to TEC perturbation (dTEC), see equation (11) in the next section.

3.1 Fitting tool: Singular Spectrum Analysis (SSA)

Different order of polynomial fittings as a band-pass technique to filter out diurnal variability and TEC perturbations associated with MSTIDs have been used in previous studies (Ding et al., 2004; Wang Min et

al., 2007; Valladares and Hei, 2012; Jonah et al., 2016). However, most of these techniques have some limitations because the direction of the trend of the fitness line and degree of smoothness/resolution cannot be controlled due to imposition of predetermined function. This is the reason we adopted singular spectrum analysis (SSA) algorithm as a detrending tool for dTEC. Our choice of SSA (see equation 7-10) among other things is because it is a nonparametric spectral estimation method for time series which cannot be affected by the limitations described above and most importantly due to its ability to find trends of different degrees of resolutions. We use equations (7) to (10) to map the original one-dimensional TEC time series (i.e. FN) of length N into a multi-dimensional series of lagged vectors of size L, where N is greater than two.

$$\overbrace{f_1,\ f_2,\ f_3,\ \ldots\ldots\ldots,f_L}^{window},\ f_{L+1},\ \ldots\ldots,\ f_N,\ implies\ \boldsymbol{F_1}^{T}=(f_1,\ f_2,\ f_3,\ \ldots\ldots\ldots,f_L) \tag{7}$$

$$f_1,\ \overbrace{f_2,\ f_3,f_4\ \ldots\ldots\ldots,f_L,\ f_{L+1}}^{window},\ \ldots\ldots,\ f_N,\ implies\ \boldsymbol{F_2}^{T}=(f_2,\ f_3,\ f_4,\ \ldots\ldots\ldots,f_{L+1}) \tag{8}$$

$$f_1,\ f_2,\ \overbrace{f_3,f_4,f_5\ldots\ldots\ldots,f_L,\ f_{L+2}}^{window},\ \ldots\ldots,\ f_N,\ implies\ \boldsymbol{F_3}^{T}=(f_3,\ f_4,\ f_5,\ \ldots\ldots\ldots,f_{L+2}) \tag{9}$$

$$F=[F_1,F_2,F_3,F_4,\ldots\ldots F_K]=\begin{pmatrix} f_1 & f_2 & f_3 & \ldots\ldots f_K \\ f_2 & f_3 & f_4 & \ldots\ldots f_{K+1} \\ f_3 & f_4 & f_5 & \ldots\ldots f_{K+2} \\ \vdots & \vdots & \vdots & \vdots \\ f_L & f_{L+1} & f_{L+2} & f_N \end{pmatrix},\ \begin{cases} 1<L<K \\ K=N-L+1 \end{cases} \tag{10}$$

F implies TEC time series which formed a trajectory matrix (**F**), f_i implies TEC values at each epoch of each PRN as time increases, and f_i must not be series of zeros, $i= 1,2\ 3,\ldots.L$. Golyandina et al. (2001) provides further details about SSA.

3.2 Estimation of TEC perturbation (dTEC) and MSTIDs event threshold

An SSA fit is determined for each TEC time series ($TEC_{SSA\text{-}fit}$) of the corresponding satellite. The TEC perturbation (dTEC) is obtained by subtracting the $TEC_{SSA\text{-}fit}$ from the TEC estimate.

$$dTEC = [\ TEC\ ] - [\ TEC_{SSA\text{-}fit}\ ] \tag{11}$$

The approach to obtain dTEC in equation (11) is known as detrending. We determine that an MSTID event is detected whenever the TEC perturbation (dTEC) points fall above the event threshold (ETH) value of 0.07 TECU (Husin et al., 2011). The choice of ETH value was based on computing the standard deviation of the

TEC perturbation (dTEC) of all epochs per observed satellite (Warnant, 1998; Warnant and Pottiaux, 2000). We iterated the entire standard deviation process for several satellites for different days and then found an approximate value of the most dominant standard deviation value which we set as the ETH point value.

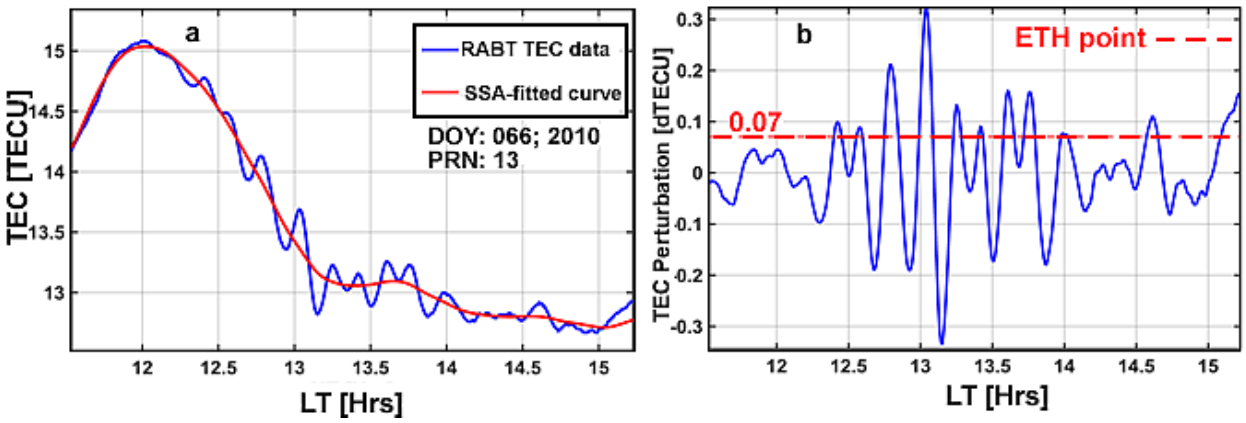

Fig. 3 (a) TEC time series in PRN 13 as observed at RABT GPS station exhibiting wave-like structures depicting to be MSTIDs. The red line fitted curve ($TEC_{SSA\text{-}fit}$) is the background trend while (b) is the corresponding detrended TEC time series known as dTEC.

3.3 Determination of MSTIDs Characteristics

In this study, we define MSTIDs as the dTEC that satisfy the following criteria: (1) the dTEC has as amplitude exceeding 0.07 TECU (1TECU=10^{16} Electron/m^2) (Fig. 3b); (2) the horizontal wavelength is described as the distance between peak to peak of each wave event using visual assessment of dTEC signals (Jonah et al., 2016) and estimated to be less than 500 km; (3) the dTEC series was transformed from the time domain to the frequency domain in order to determine the event dominant period using a Fast Fourier Transform (FFT) (Husin et al., 2011; Hernández-Pajares et al., 2012) and the period is estimated to be less than 60 mins; (4) the propagation velocity does not exceed 450 m/sec and the propagation direction is southward (equatorward); see equations (13) and (14). The geometry of calculating the MSTIDs propagation parameters is plotted in Fig. (2b) as an illustration in determining the azimuth and velocity. It must be noted that GPS receiver stations that are relatively close to each other are considered to form a sub-network (minimum of three stations) following the approach of Afraimovich et al. (1998); Hernández-Pajares et al. (2012); Valladares and Hei, (2012); and Habarulema et al. (2013a). Hence, we form two sub-networks; N1 (RABT-TETN-IFR1) and N2 (ALX2-NICO-RAMO) as seen in Fig.1. The GPS receiver stations RABT, TETN and IFR1 represented by X, Y and Z respectively in Fig 2(a-b) form N1. We assume that the TID's wavefront propagates along the Earth's spherical surface and crosses point positions X, Y and Z with speed $\boldsymbol{v}$ and propagation azimuth (ϕ). The azimuth is measured from the north (**N**) towards the east along the horizon. The phase fronts propagation velocity satisfies the equations below (Ding et al., 2007).

$V\Delta t_1 = \Delta S_1 \cos(\Phi - \psi_1)$, $V\Delta t_2 = \Delta S_2 \cos(\Phi - \psi_2)$, (12)

Where Δt_1 and Δt_2 are time delays for dTEC to move from point X to Y and Z respectively along the Earth spherical surface and computed using cross-correlation. ΔS_1 is the spherical distances between X and Y, ΔS_2 is the spherical distance between X and Z, while ψ_1 and ψ_2 are the azimuths of spherical paths XY and XZ.

$$\Phi = \arctan\left(\frac{\Delta t_1.\Delta S_2.\cos\psi_2 - \Delta t_2.\Delta S_1.\cos\psi_1}{\Delta t_2.\Delta S_1.\sin\psi_1 - \Delta t_1.\Delta S_2.\sin\psi_2}\right) \quad (13)$$

Phase velocity of the TIDs was computed using

$$V = \frac{\Delta S_1}{\Delta t_1}\cos(\Phi - \psi_1) \quad (14)$$

Different observation points of X, Y, and Z were chosen to compute absolute values of V and Φ; thereafter we take the average value of V and Φ as the MSTIDs propagation velocity and azimuth. One important criterion that must be noted for computation of azimuth using equation (13) is that each of the GPS receiver stations within a sub-network must see the same satellite per observation time. Hence, the same satellite that could be seen by a sub-network is filtered for computation while other satellites are discarded. We also calculated the MSTIDs percentage occurrence rate (POR) of the event using equation (15).

$$POR = \left[\frac{\alpha}{\omega}\right] x\,[100] \quad (15)$$

where α is the total count number of dTEC estimation above ETH per epoch, ω is the total count number of dTEC estimation per epoch.

4.0 Results

We have analyzed the derived dTEC in the North African region during 2008-2016 and the wave-like structures depicted to be MSTIDs were estimated. The MSTIDs percentage occurrence rate (POR) was determined and divided into hourly bins. Variations in local time (LT) are analyzed by sorting the data into one hour bins. Following Jayawardena et al. (2016) and Wang et al. (2017), we considered the daytime (DT: 0600–1800 LT) as dawn to dusk while the nighttime (NT: 1800–0600 LT) as dusk to dawn. However, for easy analysis and convenience, we converted the LT to universal time (UT) in a case where MSTIDs event are being observed simultaneously at more than one station. MSTIDs are observed and their characteristics are determined. Fig.4 shows an illustration for the case of a single day.

4.1 Observation of MSTIDs during 07 March 2010

In this section we determine the MSTIDs characteristics for 7th March 2010 (DOY 066) using equations (12), (13), and (14).

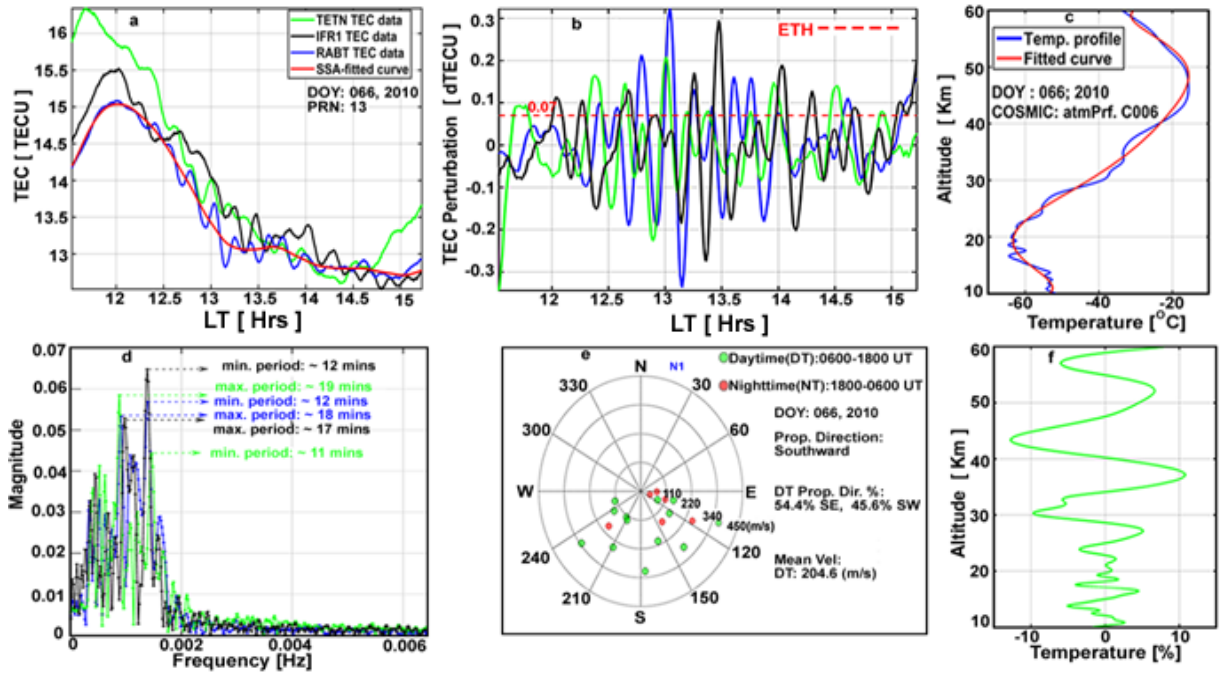

Fig. 4 (a) TEC versus UT measured by the N1 GPS receivers; color green, black and blue signal traces represent TEC values from the three receivers and the red lines represent the estimated background/unperturbed TEC values. (b) Corresponding detrended TEC time series of fig. (a), (c) Perturbed temperature profile from COSMIC satellite (blue color) and its fit (red color), (d) MSTIDs minimum and maximum dominant periods, (e) N1 polar plot representing MSTIDs velocities and azimuth for daytime during DOY 066 (f) Signature of upward AGW propagation obtained from the detrended temperature profile in fig. (c).

The TEC time series exhibited continuous fluctuations as observed in PRN 13 at different local times (LT) in different stations of the N1 network. The DOY 066 daytime phenomenon in Fig. 4a has majorly been assumed to be caused by AGW as stated in the introductory section. Fig.4c is an example showing a potential link between AGW-MSTIDs as well as excitation mechanism of daytime MSTIDs occurrences due to AGW passage. The AGW passage evidence is exhibited in the temperature profile which shows some fluctuations and perturbation effects that eventually got above 50 km into the ionosphere and directly impacted it (Azeem and Barlage, 2017). We use temperature profile measurement within the geographic coordinate area that is close to the stations under investigation. Minimum and maximum dominant period of MSTIDs is obtained using FFT and it is computed to be an average of 11.7 mins and 18 mins, respectively. Fig.4 (e) shows that MSTIDs propagates towards the equator (southward) but indicated a higher percentage towards the south-east (SE). The temperature profile is detrended, in line with Wang and Alexander, (2009),

describing the output structure to be the vertical signature of upward AGW propagation. Fig.4(f) exhibited an increase in amplitude with height and it is a major characteristics of AWG (Jonah et al., 2016).

4.2 Two-dimensional observation of MSTIDs over North Africa

Fig.5 shows the two-dimensional maps of MSTIDs over North Africa region at selected times during 1019 to ~1200 UT (daytime) of day 066, 2010, using PRN 20 in all the eight stations. With careful observation Fig.5 (a-b) depicted, that TID was propagating towards the equator and south-east (SE) with maximum amplitude of 0.3 TECU. There are absences of GPS networks within certain longitudes; therefore, we split Fig.5 (a-b) into two to increase the map resolution.

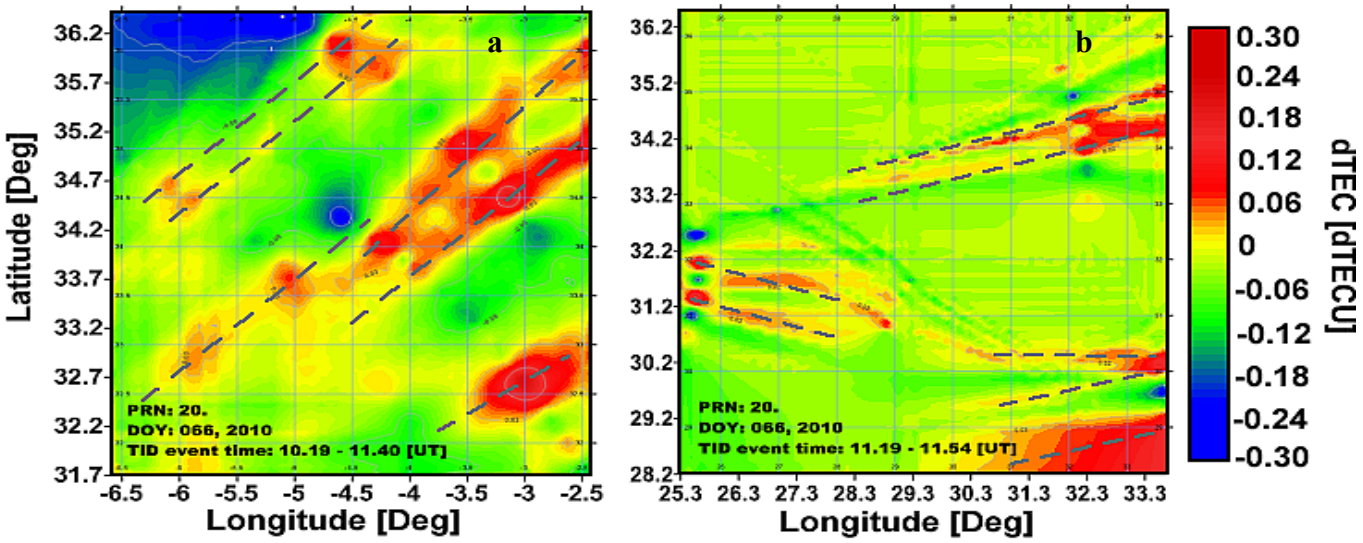

Fig. 5 Two-dimensional maps of MSTIDs over North Africa at 1019 to ~1200 UT on 7th March, 2010 (DOY 066).

4.3 Local observation of MSTIDs over selected GPS receiver stations in North Africa

Using the network geometry approach in section (2.0), we formed sub-networks N1 and N2. Fig. 6(a-c) exhibits local diurnal and seasonal variations of MSTIDs occurrence at the different stations during the period of the study. Data gap are indicated by the white portions on figure. Fig. 6(a-b) are stations located at mid-latitude stations that make up the sub-networks (N1 and N2) while Fig. 6(c) is a low latitude station (MAS1). The contour structure in Fig.6 (a-b) exhibited by the mid-latitude stations shows a similar pattern of MSTIDs event but is clearly different in terms of local time. Comparing the mid-latitude and low latitude (Fig.6(c)), there are clear differences in local time, seasons, and latitude. The MSTIDs occurrence shows a strong dependence on the season and different local times but with a major peak around the (nighttime) 2100-0200 LT and 1900-0200 LT in June solstice at N1 and N2 stations respectively. At low latitude

(MAS1), the major peak is around 2000-0100 LT (nighttime) in March equinox and June solstice but got extended to December solstice in 2011 and solar maximum years (2013-2014). Furthermore, both the mid-latitude and low latitude stations exhibited their respective minor peaks in December solstice (i.e. winter); around 1200–1600 LT (N1), 09000–1600 LT (N2) and 1100–1800 LT (MAS1). At N1 and N2, the maximum MSTIDs POR is observed to be between ~40 % to ~50 % in June solstice while it is seen to be between ~45 % - ~60% during June and December solstice, and equinox. There is an increase in occurrence rate with different intensity during nighttime at both Mid-latitude and low latitude. All stations exhibited an increasing MSTIDs POR consistently with the solar cycle. The highest MSTIDs POR at the Mid-latitude is consistently observed in June solstice during 2008-2016, while that of low latitude is consistently observed in June solstice during 2008-2010 and December solstice during 2011-2015. The POR density shows that the occurrence rate varies with time of the day and night as a function of latitude and it also reveals a strong nighttime MSTID occurrence dependence on latitude. This result seems to reveal occurrence variation and a level of inconsistency during day and night time from year to year.

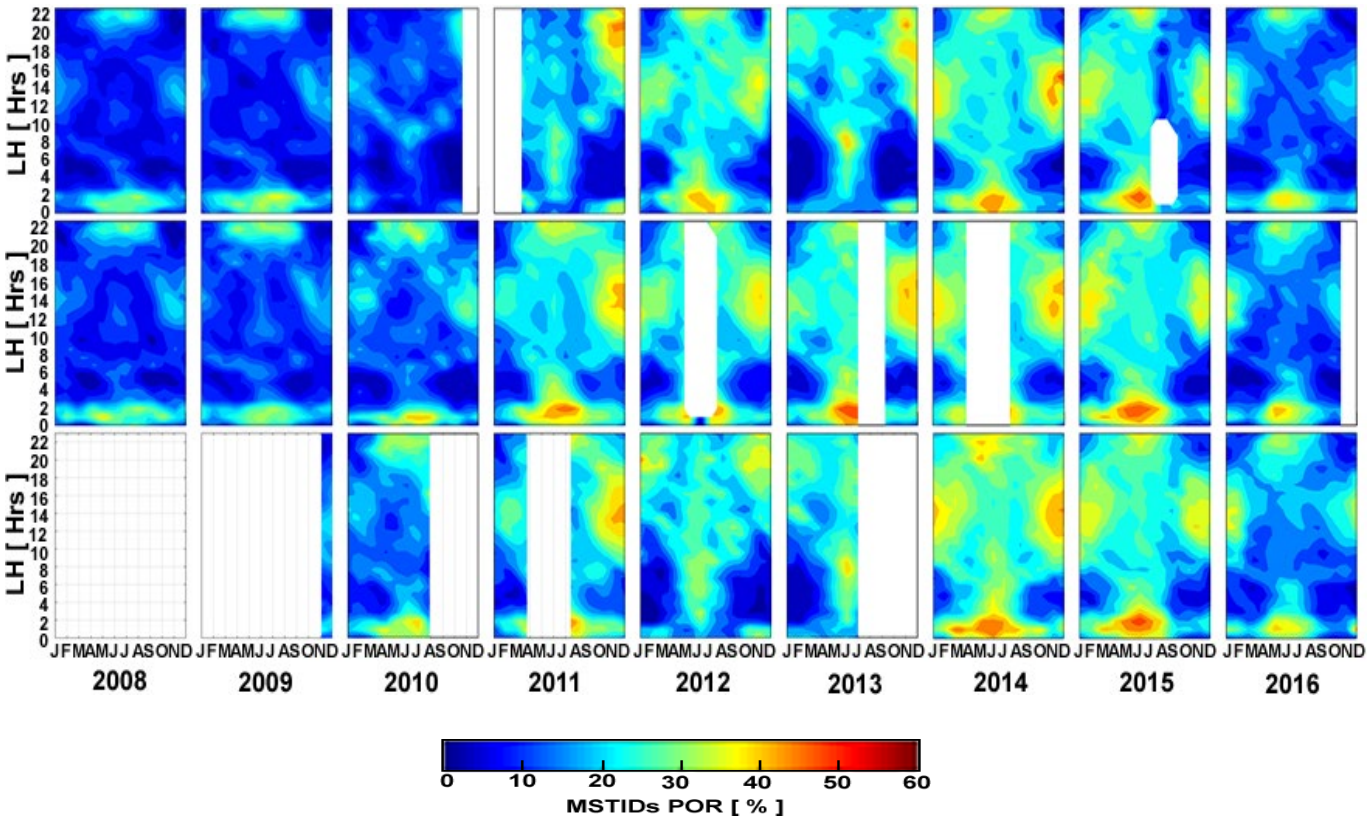

Fig. 6a: Local diurnal and seasonal variations of MSTIDs occurrence at sub-network N1 at Mid-latitude. (top panel: TETN, middle panel: RABT, bottom panel:IFR1).

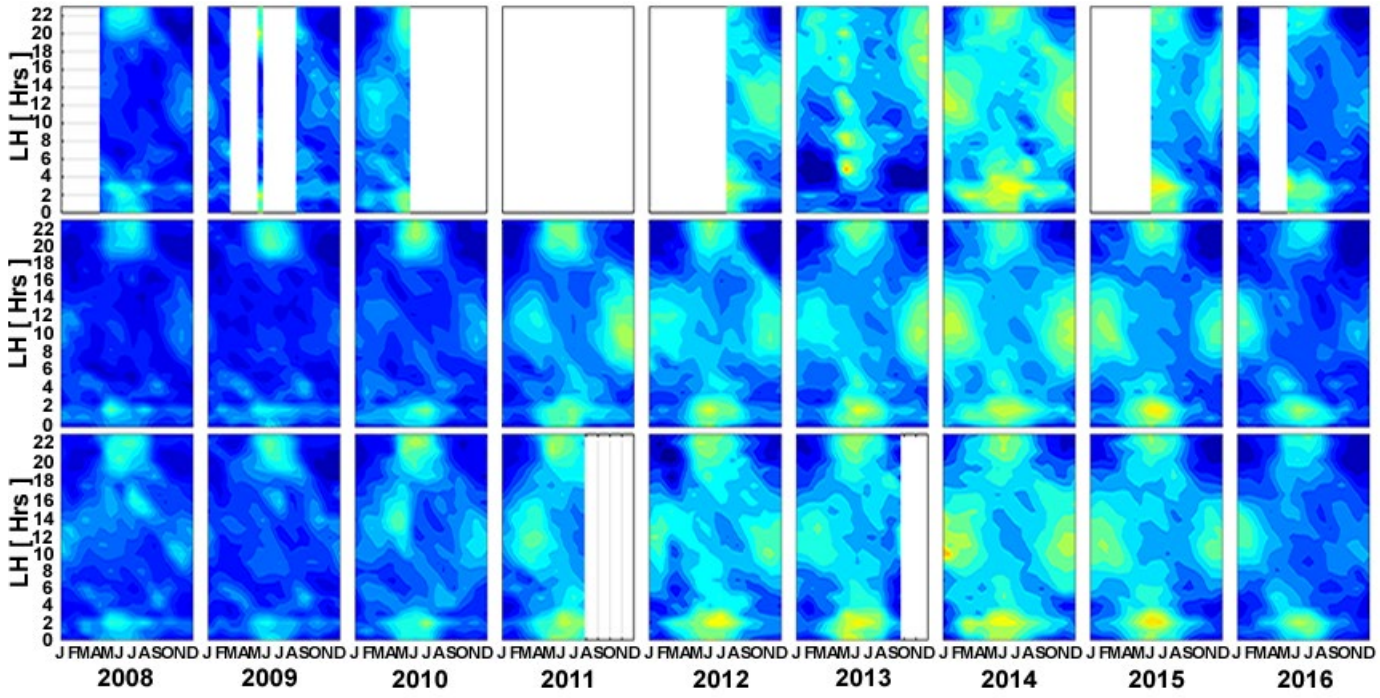

Fig. 6b: Local diurnal and seasonal variations of MSTIDs occurrence at sub-network N2 at Mid-latitude. (top panel: ALX2, middle panel: NICO, bottom panel: RAMO)

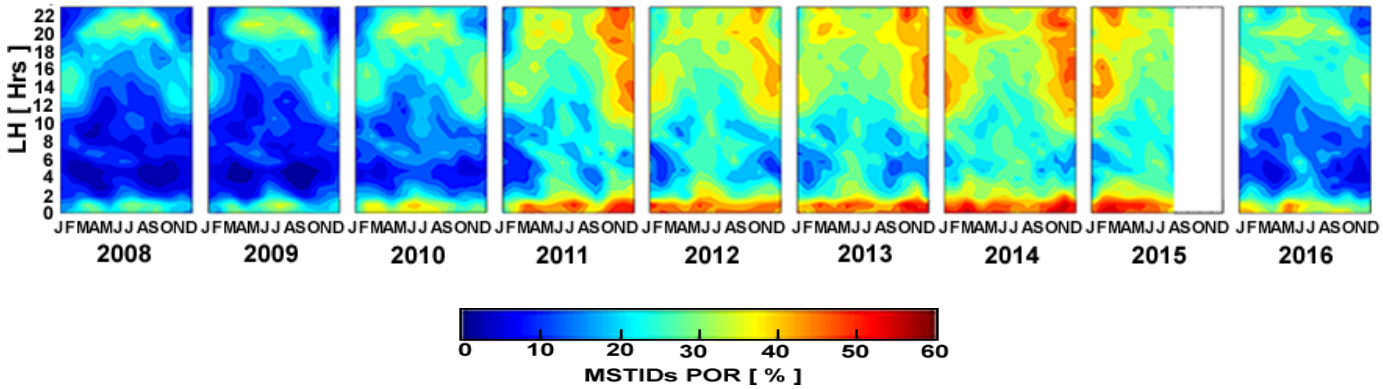

Fig. 6c: Local diurnal and seasonal variations of MSTIDs occurrence at low latitude station (MAS1)

Hence, in subsequent sections, we analyze day and nighttime amplitudes and further separate them to make a statistical count of daily maximum amplitude during day and night period.

4.4 Local and seasonal dependence of MSTIDs amplitudes

Fig. 7(a-b) shows MSTIDs daily maximum amplitudes for daytime and nighttime were separated and analyzed for both sub-networks in Mid-latitude (N1 and N2) and low latitude (MAS1). For better visual analysis and to observe slightest changes in the multiple scatter plots, we introduced a mathematical function (simple moving average) which estimates the average value to determine the trend line-curve for both day and night (red and blue line). White portions without points or trend line-cur are an indication of data gaps.

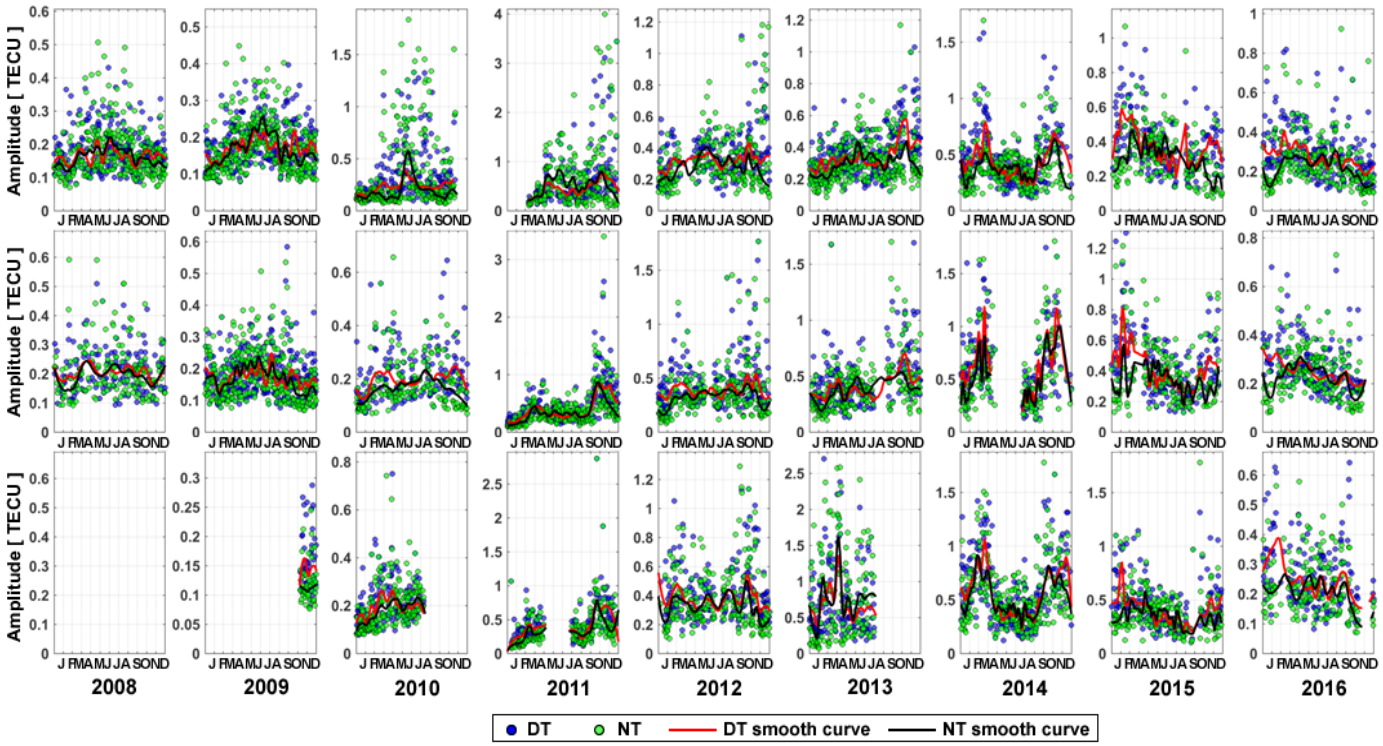

Fig. 7a: MSTIDs daily maximum amplitudes for day and night time for sub-network N1

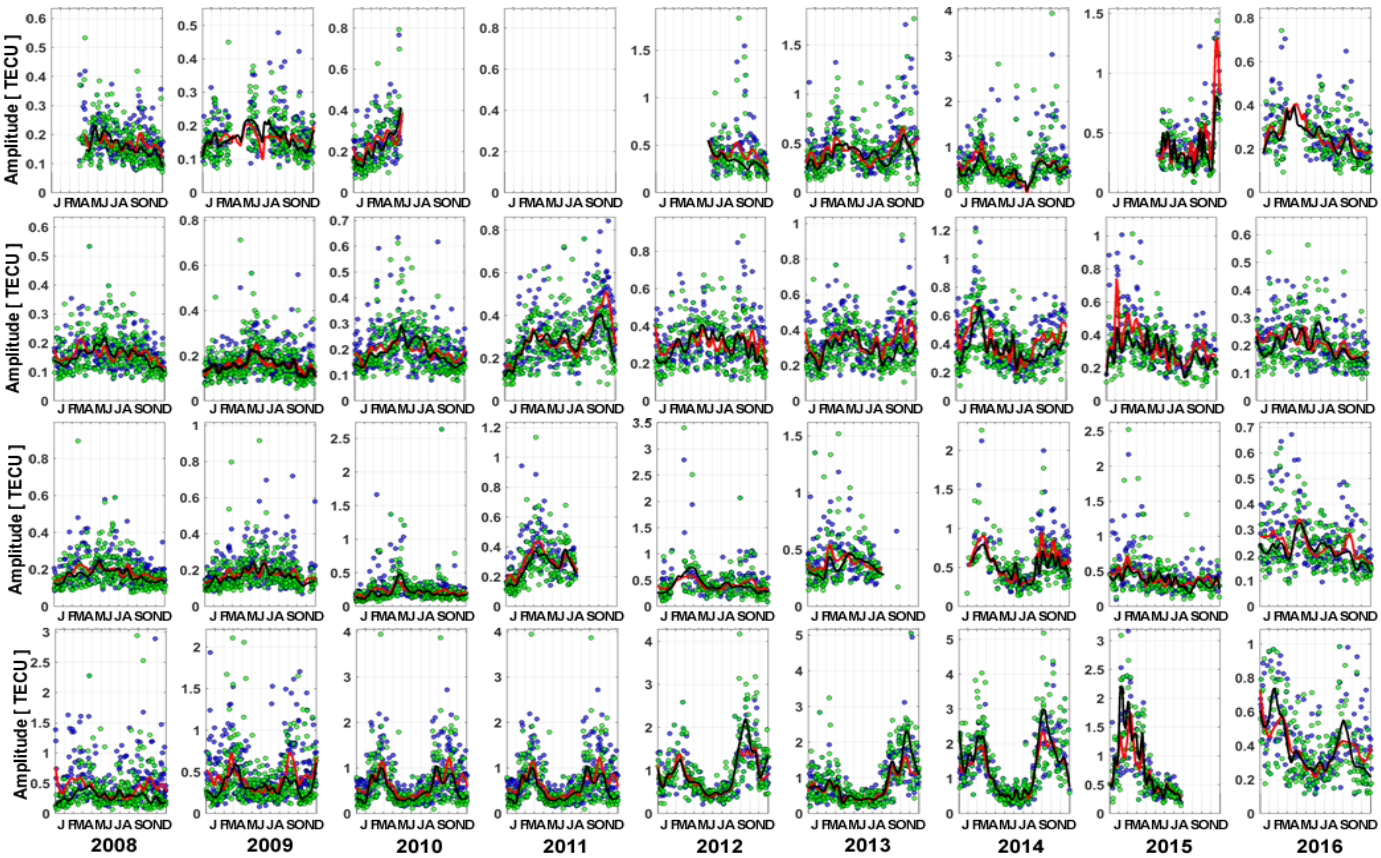

Fig. 7b: MSTIDs daily maximum amplitudes for day and night time for sub-network N2 (N2: top three panels). The fourth panel is the daily maximum amplitudes for day and night time for low latitude station (MAS1)

MSTIDs daily maximum amplitudes for daytime and nighttime were considered in this section. The daytime and nighttime amplitudes are generally high at low-latitudes compared to mid-latitude. The estimated average which forms the trend line-curve is used for analysis in this section. The amplitude trend line (i.e. smooth curve line) at low-latitudes indicated a consistent asymmetrical nature with major and minor peaks during 2008-2016. At mid-latitudes, both sub-networks N1 (Fig. 7a) and N2 (Fig.7b-top three panels) stations exhibited different local behavior in amplitude even though all stations are located within the same Mid-latitude. In N1, the amplitude exhibit major peaks around (0.24 - 0.50 TECU) at nighttime in June solstice during the minimum solar phase years (2008 - 2010). N1 exhibits major peaks around (0.6 - 0.81 TECU) at both nighttime and daytime in September equinox (minor peaks in March equinox) during 2011. Furthermore, the major peaks during 2012 -2013 is around (0.43-0.59 TECU) at daytime in December solstice. The amplitude pattern of N1 in 2014 is symmetrical, with daytime having the highest amplitude around (0.81 - 1.22 TECU) in March equinox months, while during 2015-2016 the major amplitude is around (0.39 - 0.82 TECU) at daytime in March equinox. In N1 sub-network, the dominant major amplitude is observed at daytime in the equinox months (September, October) and December Solstice (November, December). The highest amplitude during the June solstice is dominant during the nighttime at N1 sub-network. In N2 sub-network (Fig.7b-top three panels), the major peaks during the minimum solar phase years (2008 - 2010) are around (0.23 - 0.48 TECU) at nighttime in June solstice. Nighttime amplitude is consistently higher than daytime during the minimum solar phase. During the daytime in 2011, N2 (NICO) exhibits a major peak around (0.54 TECU) in December solstice (minor peaks in March equinox). In the daytime during 2012 – 2013, the major peak is dominantly around (0.38 - 0.53 TECU) in September equinox (minor peaks in March equinox) and at daytime, the amplitude is higher in 2014 than other years. The 2014 amplitude pattern is symmetrical with daytime having the highest amplitude in equinox season around (0.62 - 0.84 TECU) in the equinox months. In 2015-2016, the major peak amplitude in the daytime is observed to be around at equinox months, and it is around (2015; 0.24 - 0.50 TECU), while in 2016 the MSTIDs amplitude is around (0.28 - 0.41 TECU). In both N1 and N2, the nighttime amplitude consistently and dominantly higher than daytime during the solar minimum year (2008-2010). On the contrary, the daytime amplitude consistently and dominantly higher than nighttime during the solar minimum year. Statistically, the MSTIDs amplitudes are higher during June solstice (61%) than equinox at mid-latitudes while at the low latitude the amplitudes are higher during equinox seasons (100%) than in any other seasons. The amplitude values increase or decrease with solar cycle phases. At low-latitude, Fig.7b (last panel) shows that the MSTIDs amplitudes are generally high in equinox seasons. Considering altogether the amplitude major peaks, the amplitude during the minimum solar phase years (2008 - 2010) and ascending phase (2011) exhibit major peaks at (0.60 - 1.32 TECU) during daytime in September equinox (minor peaks in March equinox) and at (0.45 - 1.21 TECU) during nighttime in March equinox (minor peaks in September equinox). On the contrary, during the solar maximum year (2012-2014) the amplitude major

peaks at nighttime and daytime are within (2.20 – 3.00 TECU) and (1.52 – 2.30 TECU) respectively, in September equinox (minor peaks in March equinox). The amplitude dropped in 2015-2016 because the solar cycle was approaching another solar minimum year (descending phase). Thus, in 2015 – 2016, the amplitude major peaks at nighttime and daytime were within (0.71 – 2.35 TECU) and (0.58 – 1.58 TECU) respectively, in March equinox (minor peaks in September equinox). However, it must be noted that the high background TEC experienced during high solar activities in equinox season also influences the MSTIDs amplitude, in that whenever the TEC background is large, the amplitude of TEC perturbation is also large.

4.5 Annual MSTIDs characteristics

Fig. 8 shows the annual MSTIDs event count (AMEC) during 2008-2016 for which daytime (DT) and nighttime (NT) were estimated using equation (16). The event percentage was counted to quantify the event based on the solar activity (i.e. MSTIDs event counts). At low latitude, the event is consistently high at nighttime which is dominantly above 50%, compared to mid-latitudes cases where the same nighttime period were dominantly below 50% except during the solar minimum of 2008, 2009, 2010, and 2016. On the contrary, at mid-latitudes the figure shows that MSTIDs at daytime are dominantly high above 50% during 2011 – 2015 while at low latitude the daytime are consistently below 50% during daytime in 2008-2016.

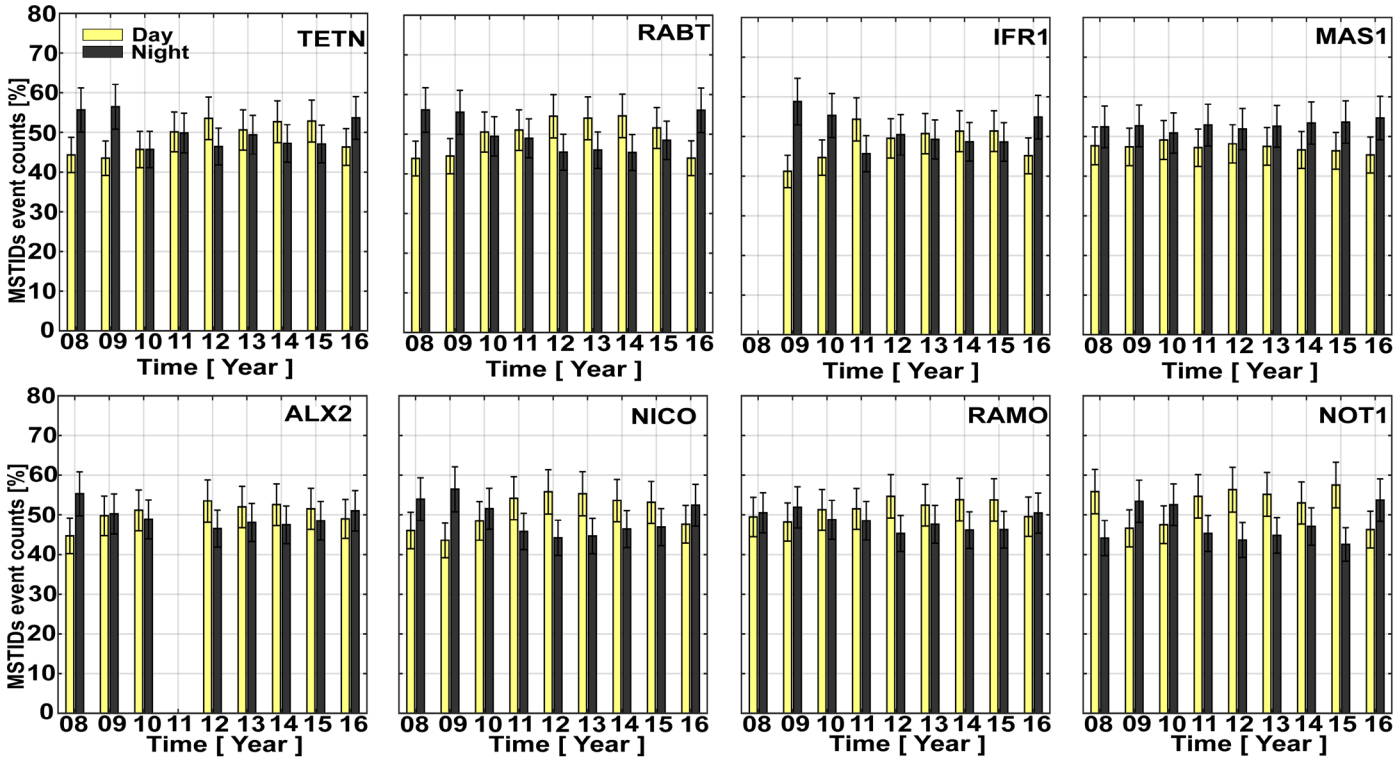

Fig. 8 Annual counts of MSTIDs occurrence in daytime and nighttime for all stations during 2008 – 2016.

$$\text{AMEC} = \left[\frac{\text{total count No. of } (\alpha) \text{ at DT during the year}}{\text{total count No. of } (\omega)}\right] \text{x } [100] \qquad (16)$$

Following equation (13) in section 3.3, we estimated MSTIDs azimuth (see fig. (9)). Fig. 9 shows plots of the annual MSTID propagation direction during daytime (DT) and nighttime (NT), and the corresponding azimuth occurrence rate in percentage on the vertical axis. To avoid azimuth points clusteredness or superimposition, and for clearer analysis, we plotted the points on a bar-chart which gives discrete cardinal directions; North (N), North-East (NE), East (E), South-East (SE), South (S), South-West (SW), West (W), and North-West (NW) following Otsuka et al. (2013) approach.

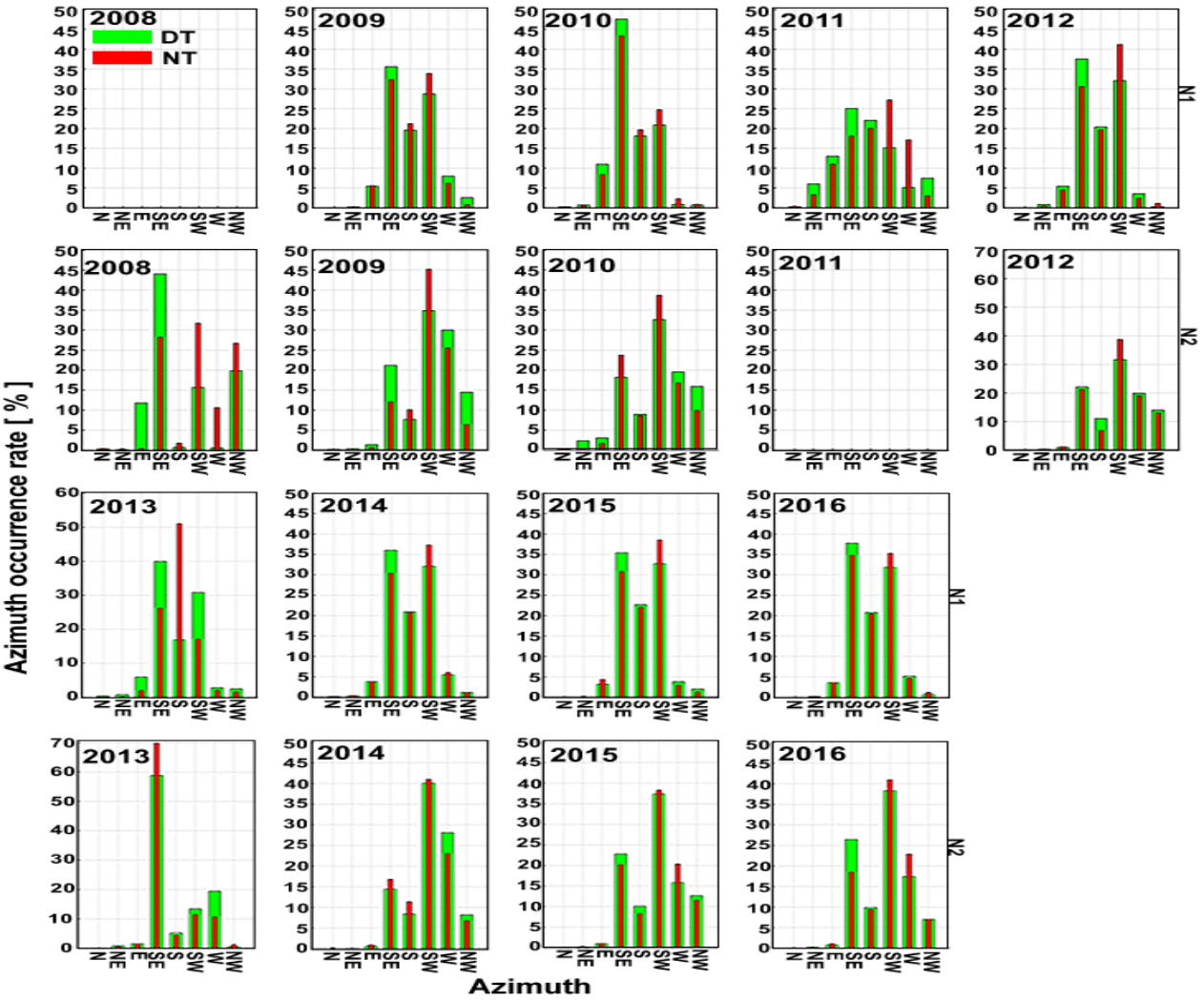

Fig. 9 Annual MSTIDs propagation direction plots for the two networks; N1 and N2.

The figure consists of four panels where first and second top panels are rows of N1 and N2 networks during 2008-2012, while the third and fourth panels are rows of N1 and N2 networks during 2013-2016. There are data gaps at IFR1 and ALX2 stations which is why N1 (2008) and N2 (2011) respectively, were not plotted. The figure reveals that MSTIDs dominantly propagate southward (equatorward) at both daytime and

nighttime. The maximum azimuth occurrence rate during 2008-2016 is: ~ 48% (SE) at daytime in 2010 and ~ 50% (S) at nighttime during 2013 in N1, while we obtain ~ 58% (SE) at daytime in 2013 and ~ 70% (SE) at nighttime during 2013 in N2. However, general observation shows that in both N1 and N2, the dominant MSTIDs propagation direction during DT is towards the south-east, while the dominant propagation direction during NT is towards the south-west. We also observed an inconsistent propagation direction in NT where MSTIDs in N2 network preferably propagate towards SE during 2013. The MSTIDs characteristics are often times obtained within certain values as stated in section (1.0), following (Hocke and Schlegel, 1996; Grocott et al., 2013). In N1 and N2 of 2008-2016, the periods were estimated from detrented TEC time series using fast Fourier transform (FFT) following (Husin et al., 2011). Periods estimated with less than 6 minutes were regarded as noise fluctuations and therefore eliminated (Valladares and Hei, (2012)). The velocities were computed using equation (14) and the wavelengths were estimated from the distance the TEC wave-like structure traveled in space (latitude or longitude) following (Jonah et al., 2016). The mean of velocity, period, and wavelength of N1 and N2nd of both daytime and nighttime of MSTIDs events during the entire study period are stated in Table 1. These values are within the ranges typically associated with MSTIDs.

Table 1. The mean characteristics of daytime and nighttime MSTIDs observed during 2008-2016.

Parameters	**DT**		**NT**	
	N1	**N2**	**N1**	**N2**
Velocity	~71 - 248 m/sec,	~217 - 333 m/sec,	~51 - 227 m/sec,	~207 - 312 m/sec
Period	~14 - 38 mins,	~16 - 35 mins,	~13 - 35 mins,	~16 - 37 mins
Wavelength	~118 - 391 km,	~128 - 373 km,	~96 - 382 km,	~109 - 361 km

Table (1) shows that NT velocity is faster than DT, while the period and wavelength do not show much disparity in both N1 and N2 cases. However, the total average of intra-distance in each of the sub-network N1 and N2 is 206 km and 508 km, respectively, and this may be probably responsible for the disparity in the average velocities result in N1 and N2. Fig.10 shows a regional distribution of MSTIDs on a spatio-temporal map over the North Africa region (mid-latitude). MSTIDs maps from different sectors at mid-latitude were superimposed. The local times (LT) was converted to UT for time uniformity, easy analysis and most importantly to observe the dominant event time of occurrence for each year covering geographic latitudes (GL) 30°N to 42°N and longitude 18°W to 42°E (Otsuka et al., 2013).

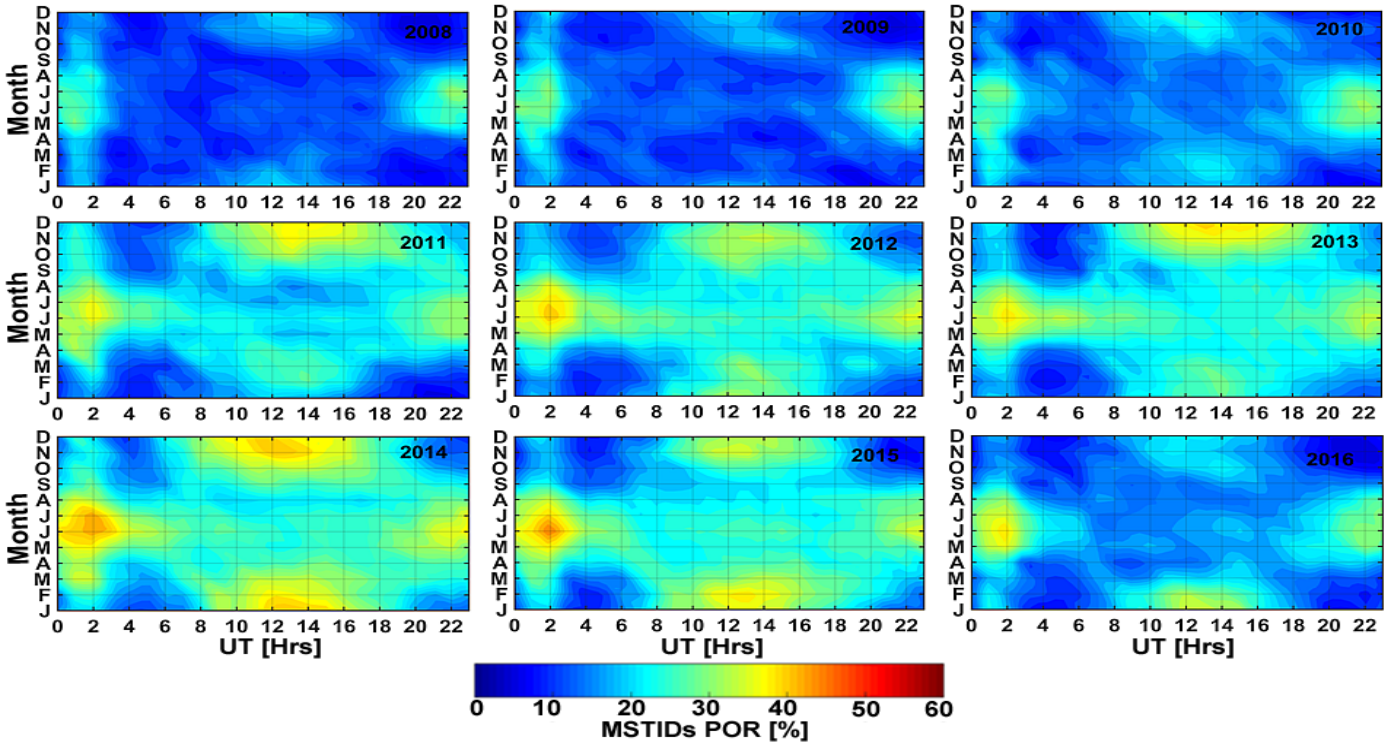

Fig. 10 Universal time and seasonal variations in MSTIDs POR at mid-latitudes (42^0N ≤GL ≥ 30^0N); 2008 – 2016

The distribution of dominance occurrence of MSTIDs in Fig. (11) shows a semiannual variation with the major primary peak at June solstice (i.e. summer) during the NT (2100 - 0300 UT) and secondary peak at December solstice (i.e. winter) during the DT (1000 - 1500 UT). The maximum MSTIDs POR was observed to be ~45% in 2014 and 2015.

5.0 Discussion

We have investigated statistically dTEC variations observed by GPS receivers located in Northern African region at mid-latitudes to reveal MSTIDs occurrence rate at local time, seasonal, latitudinal variations and propagation direction at daytime and nighttime, respectively, during 2008-2016. Our statistical results show a distinct difference between the observed MSTIDs activities. Fig. 3a and 4a showed daytime TEC measurement exhibiting wave-like structures depicting to be MSTIDs due to the passage of AGW (Hines, 1960; Hooke, 1968; Jonah et al., 2016; Oinats et al., 2016; Figueiredo et al., 2018). The AGWs passage involves vertical displacement of air parcels originating in the troposphere (Hines (1960)) and which causes perturbation in the ionospheric electron density. Temperature and wind perturbations are the two parameters that oscillate for a freely propagating wave which transport energy and momentum from their source into certain height in the ionosphere. The neutral air wind perturbation collides with the plasma at F region, and then the charged ions are set in motion but are constrained to move along the magnetic field lines. The transportation of the charged molecules/ions along the magnetic field lines leads to electron density

enhancement in certain places along the wavefront and also depletions in some other places. The continuous and regular enhancement and depletion of the plasma density consequently leads to TIDs occurrence (Hooke, 1968). Having discussed the daytime MSTIDs mechanism as being generated by AGWs, the sources of these waves include convection, typhoon and other atmospheric activities (Hines, 1960; Hooke, 1968; Kotake et al., 2007; Figueiredo et al., 2018). The observation in Fig. (4a) shows a link between AGW and MSTIDs in the investigated day, Fig. (4c) shows the daytime signature of AGW which is about the same time of observing MSTIDs and Fig. (4f) exhibits an upward/vertical propagation as amplitude increases with height which is assumed to be a major characteristic of AGWs. Our result in Fig 4(a-f) shows agreement with the results obtained by Jonah et al. (2016) who worked on the Southern hemisphere of the Brazilian sector. The MSTIDs 2-D map in Fig. 5 (a-b) exhibited a wave-like structure with the wavefronts stretching from the North (N) towards the South-southeast (SE) with the wavefronts between ~42 – ~250 km, with maximum amplitudes peak value of 0.30 TECU. The wave-like structures can be identified as daytime MSTIDs which are due to AGWs, and its excitation mechanism was already discussed above. By visual assessment, we carefully compared the wave structures in Fig. 5a and Fig. 5b and it can be observed that the wave structure in Fig. 5a seems stronger and well transverse than in Fig. 5b. The wave is getting decay already as seen in Fig. 5b and preferred to propagate in different direction. The propagation source of the AGW seems to be located in the far North of the mid-latitude but seen propagating southward and mainly towards the south-east. Fig. 6 (a-c) shows different characteristics between daytime and nighttime MSTIDs, such as local time dependence, seasonal dependence, latitudinal dependence, and solar activity dependence. These facts indicate that mechanisms causing MSTIDs could be different between daytime and nighttime period, and from location to location. A high occurrence rate of MSTIDs was observed during the daytime 1100–1600 LT, 0900–1400 LT, and 1100–1800 LT, at N1, N2 and MAS1 station, respectively. There is variability in the MSTIDs nighttime event due to latitudinal dependency, but the highest MSTIDs occurrence rate were observed during June solstice (May–July) in every year at mid-latitude (N1; ~2100 - ~2300 LT and N2; ~1900 - ~2300 LT). There is different MSTIDs occurrence behavior as seen in Fig (6c; low-latitude), where the MSTID nighttime event (2000-2300 LT) oscillate between March equinox (February, March, and April) and June solstice during 2008-2010, while the nighttime activities become weaker in June solstice but becomes high in December solstice (November, December, and January) during 2011-2015, and in 2016 the high occurrence rate at nighttime switch back to June solstice. Furthermore, the MSTIDs again experiences an high occurrence rate during the local time (nighttime) within the range of 0001-0200 LT and 0001-0300 LT in June solstice at N1 and N2 respectively, while at MAS1station, the high occurrence rate was recorded during the local time (nighttime) 0001-0100 LT in March equinox and June solstice (2008-2010), and spans through March equinox, June solstice and winter (2011-2015). It must be noted that the increase in MSTIDs occurrence rate from year to year is relative, and the increase in occurrence rate of MSTIDs as observed increases with solar cycle. Our results show good agreement with

the MSTIDs nighttime results over South-East Asian sector (Japan) reported by Tsugawa et al. (2006), although there is little difference of the level of occurrence in the nighttime within the local time range of 0001-0300 LT. Our results show better agreement with results obtained for the North America sector (California) (Hernández-Pajares et al., 2012). MSTIDs exhibited a significant increase in the year 2011, relative to 2009 and 2010, most especially during December solstice, probably due to an ascending solar phase year. The increase in December solstice may be attributed to the increase in solar activity as expressed by an increase in sunspot numbers. The average annual values of sunspot numbers from solar minimum to ascending phase are 3.1, 16.5, and 55.7 for 2009, 2010 and 2011, respectively (see. http://www.sidc.be/sunspot-data/) (Tariku (2015)). According to the POR scale in Fig. 6 (a-c), the MSTIDs occurrence rate expressed as a percentage at low latitude are higher than at mid-latitudes, most especially at nighttime. This latitudinal difference of the MSTIDs is due to the different occurrence of excitation mechanism during daytime and nighttime. The daytime results are similar to the daytime result of MSTIDs studies over North America and Southern California, conducted by Tsugawa et al. (2007). In Fig. 7 (a-b), the MSTIDs' amplitude is larger at low latitude than mid-latitude, and this is due to TEC background that is generally large at low latitude than mid-latitude. The equinoctial asymmetry nature of TEC background features in low latitude has been attributed to neutral atmospheric and $[O]/[N_2]$ ratio composition (Kherani et al., 2013). The major factor responsible for the high amplitude of TEC background is the fact that the geomagnetic latitude of MAS1 falls within EIA-region where is an upward E x B drift plasma during daytime (Bolaji et al., 2012) driven by F-region electrodynamics processes (Oluwadare et al., 2018). In addition, the nighttime amplitude peak points are dominantly higher than the daytime amplitude peak and these have been attributed to increased dissipation due to enhanced ion drag in the daytime (Hocke and Schlegel, 1996). The results obtained have shown that the TEC amplitudes increase with an increase in solar activity and the result is in agreement with Fukushima et al. (2012) and Oinats et al. (2016). In Fig. 8, the annual MSTIDs event count (AMEC) at nighttime in low latitude is high and it's consistent irrespective of solar cycle phase condition, and this might indicate that there are more electrodynamics processes within this region as discussed above. On the contrary, the AMEC is high at nighttime only during solar minimum at mid-latitude; the result is in close agreement with Ding et al. (2011) who studied MSTIDs climatology over central China in South-East Asian sector during the 2010 solar minimum. The high AMEC results at daytime during solar maximum at mid-latitude are in close agreement with Oinats et al. (2016), who studied MSTIDs statistical characteristics using radar data over East Asia (Hokkaido-F region) and European-Asian sector during the 2013-2014 solar maximum and found that MSTIDs occurrence rate is dominantly high at daytime. The figure also shows that there were more daytime events than nighttime events at mid-latitude and statistically the figure has revealed that daytime MSTIDs is a major ionospheric irregular phenomenon at Mid-latitude. The daytime MSTIDs seemed to be related to the solar terminator (Hernandes-Pajares et al., 2006, Husin et al., 2011). In Fig (4e, and 5), and Fig. 9, the propagation direction of MSTIDs for both

daytime (DT) and nighttime (NT) are dominantly Southward (equatorward) from the northern hemisphere. Hence, using Otsuka et al. (2013) approach, the result shows the azimuth occurrence rate expressed in percentage to be dominantly towards the South-East (SE) and South-West (SW) during DT and NT, respectively. Heisler, (1963) stated that propagation direction of TIDs is towards the ionospheric part where it is mostly illuminated by the Sun (from the Northern hemisphere) but the most supported theory is still in the direction of the geomagnetic field lines (Thome, 1964). At the F-regions, the ions move and travel along the geomagnetic field lines through neutral-ion collision, with a velocity the same as the velocity of the neutral motion along the geomagnetic field caused by the gravity waves (Hines, 1960; Hooke, 1968). However, the motion of the ions across the magnetic field line is constrained to move along the magnetic field lines because the gyro-frequency of the ions is much higher than the frequency of the ion-neutral collisions. The direction of the motion of the ions consequentially leads to directivity in the response of the electron density variations to the gravity waves. This kind of directivity phenomena could be responsible for daytime MSTIDs Southward propagation direction. Besides, an anisotropic frictional ion drag force has been thought to also contribute to the Southward tendency of the daytime MSTID propagation direction (Liu and Yeh, 1969; Kelley and Miller, 1997). Although on a general view, statistical result reveals that propagation direction is dominantly southward but the daytime MSTIDs is dominantly to the South-East (SE) while nighttime result is dominantly towards the South-West (Afraimovich et al., 1999; Ding et al., 2011; Hernandez-Pajares et al., 2012). The mechanisms of both daytime and nighttime MSTIDs are different from each other. The nighttime MSTID were initially discovered to be associated with increases in the F-region peak electron density altitude by Behnke (1979) and its source was conventionally assumed to be generated by electrodynamical forces such as Perkins instability (Perkins, 1973; Kelley and Fukao, 1991; Kelley and Miller, 1997; Garcia et al., 2000; Tsugawa et al., 2007; Otsuka et al., 2007). Perkins created a mid-latitude ionospheric model that finds a way around solving the complexity of the mid-latitude ionosphere. In his model he solved the momentum equations by integrating quantities along the magnetic field line and under certain conditions found the existence of unstable modes when a North-South electric field or Eastern neutral wind existed, and consequently, a pre-existent irregularity will grow with wave-fronts oriented from North-West to South-East in the Northern Hemisphere (Perkins, 1973). These instabilities are often strong in the nighttime and can generate local polarization electric field that can move the plasma upward (downward) via the E x B drift, which consequently causes perturbation in the plasma density. It must be noted that the growth rate of the generative mechanism of Perkins instability at mid-latitudes is very low and therefore would require additional seeds such as gravity waves (Hunsucker, 1982; Huang et al., 1994) as well as electrodynamic coupling processes between F- and E- regions to boost the low Perkins growth rate to allow for the MSTIDs development (Cosgrove, 2004; Otsuka et al., 2007; Yokoyama and Hysell, 2010). The Perkins instability theory is responsible for the peak of nighttime MSTIDs at the June solstice which is inversely proportional to the neutral density. It also predicts the

MSTIDs alignment with respect to the background magnetic field, but it incorrectly predicts the direction of phase front (Perkins, 1973). Both the daytime and nighttime MSTIDs statistical results of propagation direction of this study are consistent with previous studies (Jacobson et al., 1995; Kotake et al., 2007; Otsuka et al., 2011; Ding et al., 2011; Hernandez-Pajares et al., 2012; Jonah et al., 2016). However, as AGW propagate during the day, it sometimes extends to the night, while the electrodynamic coupling processes may only take place at night. Moreover, the nighttime MSTIDs may be jointly generated by AGW and electrodynamics coupling processes (Chen et al., 2019). The other non dominant propagation direction in both N1 and N2 shows that MSTIDs can propagate in any direction depending on background conditions following Valladares and Hei, (2012). In addition, the unconventional propagation directional preference might be influenced by the background thermospheric wind (Husin et al., 2011). The results in Table 1 for both the nighttime and daytime MSTIDs event exhibits typical properties of MSTIDs (Samuel, 1974; Ogawa et al., 1987; Grocott et al., 2013) and results are similar to the results over North America (Califonia) conducted by Hernandez-Pajares et al. (2012) and Tsugawa et al. (2007). In (Fig. 10), map from each station at mid-latitude are combined in order to have a general view of MSTIDs North Africa region distribution. To avoid confusion and complex interpretation the local time (LT) from each station was converted to universal time (UT). Hence, the MSTIDs region distribution map is developed. The same nighttime/daytime mechanism explained above for Perkins instability theory is also responsible for the regional distribution. The regional distribution has similar season and time (hrs) of occurrence as Fig. (6a-c) but with little difference in occurrence time range, seasonal and solar activity dependence. The high MSTIDs occurrence level observed during daytime and nighttime are 0900–1600 UT (December solstice (winter)) and 2000–0400 UT (June solstice (summer) respectively, in each year but the seasonal peak got extended to March equinox in 2014. The figure shows a consistent increase in MSTIDs occurrence with increase solar activity in June solstice. It must be noted that the COSMIC-RO observation points do not always coincide with the geographical study area and this fact is a limitation of the COSMIC satellites. Therefore, temperature profile data from sounding of the Atmosphere using Broadband Emission Radiometry (SABER) may be combined with RO data in order to fill RO gap between 60 – 90 km altitude for the study of temperature perturbation behavior and for the analysis of AGW signature at different scales into higher altitudes for more investigation of daytime MSTIDs. This investigation can be carried out in the future work.

Conclusions

For the first time, the climatology of MSTIDs has been studied during solar cycle #24 (2008-2016) using the GPS network within the North African sector at the Northern Hemisphere. Quiet days with Kp $\leq$ 3 were considered in this study. We examined the MSTIDs occurrence rate, statistical characteristics for daytime and nighttime, the excitation mechanism and spatial-temporal distribution. The study concluded that:

1. From the estimated TEC data, we derive the TEC perturbations (dTEC) by subtracting the TEC time series from corresponding best fitted ($TEC_{SSA\text{-}fit}$) obtained from non-parametric models such as SSA as a band-pass technique to filter out TEC perturbations associated with MSTIDs.

2. MSTIDs have the ability to propagate over long distances. Hence, MSTIDs have been observed by both short and long baseline measurements as in the case of N1 and N2 sub-networks and Fig. 5(a-b).

3. MSTIDs occurrence is a local phenomenon and its occurrence rate is majorly dependent on LT, season and latitude. However, we found that MSTIDs occurrence rate during study period can categorized into different groups based on location. As for location around North-West (N1) and North-East (N2) of Mid-latitude, the daytime MSTIDs is dominantly occur around (N1: 1400–1600 LT) and (N2: 1000–1400 LT) in December solstice, while nighttime dominantly occur around (N2: 2200–0200 LT) and (N2: 2000–0200 LT) in June solstice. At low latitude, the daytime MSTIDs is dominantly occur around 1300–1600 LT in December solstice, while nighttime dominantly occur around 2000–0100 LT in March equinox and June solstice during solar minimum, but get extended to September equinox and December solstice during solar maximum.

4. There is a possible connection between the observed MSTIDs and gravity waves having examined wave-like structure of TEC and a perturbed temperature profile during daytime on a selected day (7^{th} March 2010). We deduce from the analysis that AGW may be responsible for the excitation mechanism for daytime MSTIDs event of that day. There is a clear observation of upward propagation of AGW from lower atmosphere to upper atmosphere.

5. MSTIDs occurrence rate were observed to increase with increase in solar activity.

6. The results reported here show that both daytime and nighttime MSTIDs over North African dominantly propagate southward (equator).However, MSTIDs dominantly propagate towards the south-east (SE) during daytime and towards the south-west (SW) during nighttime. MSTID direction of phase front is not 100% towards the SW/SE as some propagate towards other cardinal direction.

7. The mean phase velocity in nighttime is higher than daytime; also the wavelength result in N2 is higher than N1. Despite disparity in N1 and N2 results (velocity and wavelength), the estimated results are in agreement with previous study and reports

8. There is a consistent symmetrical effect of MSTIDs amplitude at both nighttime and daytime in low latitude, irrespective of solar cycle phase with major and minor peaks equinox months. There is dominant annual asymmetry effect of MSTIDs in June solstice during solar minimum in mid-latitude with nighttime amplitude higher than daytime. The mid-latitude regional distribution of the MSTIDs activity shows a primary peak during June solstice and secondary peak during December solstice.

Abbreviations

MSTIDs: medium-scale traveling ionospheric disturbances; GPS: Global Positioning System; AGW: Atmospheric Gravity Waves; TEC: Total Electron Content; dTEC: TEC perturbations; NNSS: Navy Navigation Satellite System; SuperDARN: Super Dual Auroral Radar Network; HF: High frequency; COSMIC: Constellation Observing System for Meteorology, Ionosphere, and Climate; OR: occurrence rate; LEO: low Earth orbit; CDAAC: COSMIC Data Analysis and Archive Center; DCB: differential code biases; VTEC: vertical TEC; SSA: singular spectrum analysis; FFT: fast Fourier transform; POR: percentage occurrence rate; LT: local times; UT: universal time; DT: daytime; NT: nighttime; AMEC: annual MSTIDs event count

Availability of data and materials

The datasets generated and/or analysed in support of the findings of this study are available upon request from the corresponding author.

Competing interests

The authors declare that they have no competing interests.

Funding

This work was financially supported by the Advance Technologies for Navigation and Geodesy (ADVANTAGE) project (grant number: ZT-0007) funded by Helmholtz-Gemeinschaft, Germany.

Authors' contributions

Oluwadare T Seun performed data processing, MSTIDs estimation, MSTIDs statistical analysis, discussed the MSTIDs mechanisms and drafted the manuscript. Norbert Jakowski and Cesar E. Valladares elaborated on MSTIDs mechanism and propagation direction respectively. Andrew O. Akala, Oladipo E. Abe, Mahdi M. Alizadeh, Harald Schuh participated in the interpretation of the MSTIDs results, proper use of technical language and sequential arrangement of manuscript text structure. All authors have contributed to the work of Oluwadare T Seun.

Acknowledgments

The authors thank the International GNSS Service (IGS), University NAVSTAR Consortium (UNAVCO), The Centre d'Etudes Alexandrines, Egypt, The African Geodetic Reference Frame (AFREF), and Constellation Observing System for Meteorology, Ionosphere, and Climate (COSMIC) for preserving the raw data and make it available for scientific uses. We also acknowledge the financial support from ADVANTAGE project (grant number: ZT-0007) funded by Helmholtz-Gemeinschaft, Germany.

Authors' information

Oluwadare Temitope Seun.
German Research Centre for Geosciences GFZ, Telegrafenberg, D-14473 Potsdam, Germany.
oluwa@gfz-potsdam.de , temitopeseun@yahoo.co.uk

References

Afraimovich E L, Palamartchouk K S, Perevalova N P (1998) GPS radio interfereometry of travelling ionospheric disturbances. J. Atmos. Sol. Terr. Phys., 60, 1205– 1223

Afraimovich E L, Boitman O N, Zhovty E I, Kalikhman A D, Pirog T.G (1999) Dynamics and anisotropy of travelling ionospheric distances as deduced from transionspheric sounding data. Radio Sci., 34, 477-487

Azeem I, Barlage M (2017) Atmosphere-ionosphere coupling from convectively generated gravity waves, Advances in Space Research. Pages 1931-1941, doi.org/10.1016/j.asr.2017.09.029

Bagiya M S, Joshi H P, Iyer K N, Aggarwal M, Ravindran S, Pathan B M (2009) TEC variations during low solar activity period (2005–2007) near the Equatorial Ionospheric Anomaly Crest region in India. Ann. Geophys. 27, 1047–1057

Behnke R (1979) F layer height bands in the nocturnal ionosphere over Arecibo. J. Geophys. Res., 84, 974–978, doi:10.1029/JA084iA03p00974

Bolaji O S, Adeniyi, J O, Radicella S M, Doherty P H (2012) Variability of total electron content over an equatorial West African station during low solar activity. Radio Sci. (USA) 47. doi.org/ 10.1029/2011RS004812, 2012

Chandra K R, Srinivas V S, Sarma A D (2009) Investigation of ionospheric gradients for GAGAN application. Earth Planet and Space

Chen Guanyi, Chen Zhou, Yi Liu, Jiaqi Zhao, Qiong Tang, Xiang Wang, Zhengyu Zhao (2019) A statistical analysis of medium-scale traveling ionospheric disturbances during 2014–2017 using the Hong Kong CORS network. doi.org/10.1186/s40623-019-1031-9, Earth, Planets and Space

Ciraolo L, Azpilicueta F, Brunini C, Meza C, Radicella S M (2007) Calibration errors on experimental slant total electron content (TEC) determined with GPS. J Geodesy

Ciraolo L, Azpilicueta F, Brunini C, Meza A, Radicella S M (2006) Calibration errors on experimental slant total electron content (TEC) determined with GPS, J Geodesy (2007) 81:111–120, DOI 10.1007/s00190-006-0093-1

Cosgrove R B (2004) Coupling of the Perkins instability and the sporadic E layer instability derived from physical arguments. J. Geophys. Res., 109. doi:10.1029/2003JA010295

Ding F, Wan W, Ning B, Wang M (2007) Large-scale traveling ionospheric disturbances observed by GPS total electron content during the magnetic storm of 29–30 October 2003. J Geophys Res, doi:10.1029/2006ja012013, 2007

Ding F, Yuan H, Wan W, Reid I M, Woithe J M (2004) Occurrence characteristics of medium-scale gravity waves observed in OH and OI nightglow over Adelaide (34.5°S, 138.5°E). J Geophys Res. doi.org/10.1029/2003JD004096

Ding F, Weixing W, Guirong X, Tao Y, Guanlin Y, and Jing-Song W (2011) Climatogy of medium-scale traveling ionospheric disturbances observed by a GPS network in central China, J Geophys Res. doi: 10.1029/2011JA016545

Fedorenko Y P, Tyrnov O F, Fedorenko V N (2010) Parameters of Traveling Ionospheric Disturbances Estimated from Satellite Beacon Observations in Low Earth Orbit. doi.org/10.1134/S0016793210040109

Figueiredo C, Takahashi H, Wrasse C M, Otsuka Y, Shiokawa K, Barros D (2018) Medium-scale traveling ionospheric disturbances observed by detrended total electron content maps over Brazil. J Geophys Res Space Phys 123:2215–2227. doi.org/10.1002/2017JA025021

Frissell, N.A., Baker, J., Ruohoniemi, J.M., Gerrard, A.J., Miller, E.S., Marini, J.P., West, M.L., Bristow, W.A., 2014. Climatology of medium-scale traveling ionospheric disturbances observed by the midlatitude blackstone superdarn radar. J. Geophys. Res. Space Phys. 119 (9), 7679–7697, URL: https://agupubs.onlinelibrary.wiley.com/doi/abs/10.1002/2014JA019870

Fukushima D, Shiokawa K, Otsuka Y, Ogawa T (2012) Observation of equatorial nighttime medium-Scale TID in 630nm airglow images over 7 years. J Geophys Res 117: A10324

Garcia F J, Kelley M C, Makela J J, Huang C S (2000) Airglow observations of mesoscale low-velocity traveling traveling ionospheric disturbances at mid-latitudes, J. Geophys. Res., 105, 18407–18415

Golyandina N, Nekrutkin V, Zhigljavsky A A (2001) Analysis of time series structure: SSA and related techniques. Chapman and Hall, New York

Grant, W B, Pierce R B, Oltmans S J and Browell E V (1998) Seasonal evolution of total and gravity waves-induced laminae in ozonesonde data in the tropics and subtropics. Geophys. Res. Lett. 25, 1863-6

Grocott A, Hosokawa K, Ishida T, Lester M, Milan S E, Freeman M P, Sato N, Yukimatu A S (2013) Characteristics of medium-scale traveling ionospheric disturbances observed near the Antarctic Peninsula by HF radar, J. Geophys. Res. Space Physics. doi:10.1002/jgra.50515

Guanyi C, Chen Z, Yi L, Jiaqi Z, Qiong T, Xiang W, Zhengyu Z (2019) A statistical analysis of medium-scale traveling ionospheric disturbances during 2014–2017 using the Hong Kong CORS network. doi.org/10.1186/s40623-019-1031-9, Earth, Planets and Space

Habarulema J B, Katamzi Z T, McKinnell L A (2013a) Estimating the propagation characteristics of large-scale traveling ionospheric disturbances using ground-based and satellite data. J. Geophys. Res. 118, 7768–7782.

Heisler L H (1963) Observation of moveement of perturbations in the F-region. J. Atmospheric Terrest. Phys

Hernández-Pajares M, Juan J M, Sanz J (2006a) Medium-scale traveling ionospheric disturbances affecting GPS measurements: Spatial and temporal analysis, J. Geophys. Res., 111, A07S11, doi: 10.1029/ 2005JA011474

Hernández-Pajares M, Juan J M, Sanz J, Aragón-Àngel A (2012) Propagation of medium scale traveling ionospheric disturbances at different latitudes and solar cycle conditions, Radio Sci., 47, RS0K05, doi:10.1029/2011RS004951

Hines C O (1960) Internal atmospheric gravity waves at ionospheric heights. Canadian Journal of Physics, pp. 1441–1481

Hocke K, Schlegel K A (1996) Review of atmospheric gravity waves and travelling ionospheric disturbance: 1982-1995. Max-Planck –Institute fur Aeronomie, Germany, Ann. Geophysicae, 1996

Hooke W H (1968) Ionospheric irregularities produced by internal atmo-spheric gravity waves. J. Atmos. Terr. Phys., 30, 795 – 823

Huang C S, Miller C A, and Kelley M C (1994) Basic properties and gravity wave initiation of the mid-latitude F region instability. Radio Science, 29, 395–405, doi:10.1029/93RS01669

Husin A, Abdullah M, Momani M A (2011) Observation of medium-scale traveling ionospheric disturbances over Peninsular Malaysia based on IPP trajectories. Radio Sci., 46, RS2018. doi:10.1029/2010RS004408.

Hunsucker R D (1982) Atmospheric gravity waves generated in the high-latitude ionosphere: A review, Rev. Geophys., 20, 293– 315, doi:10.1029/RG020i002p00293

Jacobson A R, Carlos R C, Massey R S, Wu G (1995) Observations of traveling ionospheric disturbances with a satellite-beacon radio interferometer: Seasonal and local time behavior. J. Geophys. Res, 100, 1653– 1665

Jonah O F, Kherani E A, De-Paula E R (2016) Observation of TEC perturbation associated with mediumscale traveling ionospheric disturbance and possible seeding mechanism of atmospheric gravity wave at a Brazilian sector. J. Geophys. Res. Space Physics, 121, 2531-2546, doi:10.1002/ 2015JA022273

Langley R (1993) GPS world, 4

Kelley M C, Miller C A, (1997) Electrodynamics of midlatitude spread F3. Electrohydrodynamic waves ? A new look at the role of electric fields in thermospheric wave dynamics. J. Geophys. Res., 102, 11,539–11,547, 1997

Kelley M C and Fukao S (1991) Turbulent upwelling of the mid-latitude ionosphere: 2. Theoretical framework. J. Geophys. Res., 96, 3747–3753

Kherani A, De-Paula E, Olusegun J (2013) Observations and simulations of equinoctial asymmetry during low and high solar activities. Presentation at a Proceeding of the Thirteenth International Congress of the Brazilian Geophysical Society, Rio de Janeiro, Brazil, August 26–29

Klobuchar, J.A., 1996. Ionospheric effects on GPS. In: Parkinson, B.W., Spilker, J.J. (Eds.), Global Positioning System: Theory and Application, vol. 1. American Institute of Aeronautics and Astronautics Inc.

Kotake N, Otsuka Y, Ogawa T, Tsugawa T, Saito A (2007) Statistical study of medium-scale traveling ionospheric disturbances observed with the GPS networks in Southern California. Earth Planets and Space 59:95–102. https://doi.org/10.1186/BF03352681

Mannucci A, Wilson B, Yuan D, Ho C, Lindqwister U, Runge T (1998) Radio science, 33, 565

Norsuzila Y, Abdullah M., Ismail M., Zaharim A (2009) Model validation for total electron content (TEC) at an equatorial region Eur. J. Sci. Res. 28 (4), 642–648.

Ogawa T, Igarashi K, Aikyo K, Maeno H (1987) NNSS Satellite observations of medium-scale traveling ionospheric disturbances at southern high-latitudes. J. Geomagn. Geoelec., *39*(12), 709–721

Oinats A V, Nishitani N, Ponomarenko P (2016) Statistical characteristics of medium-scale traveling ionospheric disturbances revealed from the Hokkaido East and Ekaterinburg HF radar data. Earth Planet and Space doi.org/10.1186/s40623-016-0390-8

Oluwadare T S, Thai C N, Akala A O, Heise S, Alizadeh, M, Schuh H (2018) Characterization of GPS-TEC over African equatorial ionization anomaly (EIA) region during 2009–2016. Advances in Space Research. doi.org/10.1016/j.asr.2018.08.044.

Otsuka Y, Onoma F, Shiokawa K, Ogawa T, Yamamoto M, Fukao S (2007) Simultaneous observations of nighttime medium-scale traveling ionospheric disturbances and E region field-aligned irregularities at mid-latitude. J. Geophys. Res., 112, A06317, doi:10.1029/2005JA011548

Otsuka Y, Suzuki K, Nakagawa S, Nishioka M, Shiokawa K, Tsugawa T (2013) GPS observations of medium-scale traveling ionospheric disturbances over Europe, Ann. Geophys., 31, 163–172

Perkins F (1973) Spread F and ionospheric currents. J. Geophys. Res., 78, 218 – 226, doi: 10.1029/JA078i001p00218

Warnant R, Pottiaux E (2000) The increase of the ionospheric activity as measured by GPS. Earth Planets Space, 52, 1055–1060, 2000

Warnant R (1998) Detection of irregularities in the total Electron content using GPS measurements - Application to a mid-latitude station. Acta Geod. Geo1'h. Hung., Vol. 33(1), 1'1'. 121-128, 1998

Samuel H F (1974) A Theory of Medium-Scale Traveling Ionospheric Disturbances. Journal of Geophysical Research vol. 79, No. 34

Tariku Y A (2015) TEC prediction performance of the IRI-2012 model over Ethiopia during the rising phase of solar cycle 24 (2009–2011). Earth Planet Sp 67, 140 (2015).

Thome G D (1964) Incoherent scatter observations of traveling ionospheric disturbance. J. Geophys. Res. 69, 4047 – 4049

Tsuda T (2014) Characteristics of atmospheric gravity waves observed using the MU (Middle and Upper atmosphere) radar and GPS (Global Positioning System) radio occultation. Proc Jpn Acad Ser B Phys Biol Sci.;90 (1):12–27. doi:10.2183/pjab.90.12

Tsugawa T, Otsuka Y, Coster A J, Saito A (2007) Medium-scale traveling ionospheric disturbances detected with dense and wide TEC maps over North America. Geophys. Res. Lett., 34, L22101, doi:10.1029/2007GL031663

Valladares C E, Hei M A (2012) Measurement of the characteristics of TID susing small and regional networks of GPS receivers during the campaign of 17-30 July of 2008. International Journal of Geophysics, 2012, 1–14, 2012

Wang L, Alexander J (2009) Gravity wave activity during stratospheric sudden warming in the 2007-2008 Northern Hemisphere winter. J. Geophys. Res., 114, doi:10.1029/2009JD011867

Wang M, Ding F, Wan W (2007) Monitoring global traveling ionospheric disturbances using the worldwide GPS network during the October 2003 storms. Earth Planet Space. doi.org/10.1186/BF03352702

Yeh K C, Liu C H (1969) Theory of Ionospheric Waves, Department Of Electrical Engineering , University Of Illinois at Urbana-Champaign Urbana. Illinois, Academic Press New York and London

Yokoyama T , Hysell D L (2010) A new midlatitude ionosphere electrodynamics coupling model (MIECO): Latitudinal dependence and propagation of medium-scale traveling ionospheric disturbances. Geophys. Res. Lett., 37, L08105, doi:10.1029/2010GL042598

Zhao B, Wan W, Liu L, Ren Z (2009) Characteristics of the ionospheric total electron content of the equatorial ionization anomaly in the Asian-Australian region during 1996–2004. Ann. Geophys. 27, 3861–3873.